EUROPEAN FUSION DEVELOPMENT AGREEMENT

EFDA–JET–PR(01)118

O.N. Jarvis and S. Conroy

Prediction/Modelling of the Neutron Emission from JET Discharges

Prediction/Modelling of the Neutron Emission from JET Discharges

O.N.Jarvis an S.Conroy[1]

EURATOM-UKAEA Fusion Association, Culham Science Centre, Abingdon, Oxon, OX14 3DB, UK
[1]INF, Uppsala University, EURATOM-VR, Box 535, 75 121 Uppsala, Sweden

Paper to be submitted for publication in PPCF

ABSTRACT

The neutron emission from the JET tokamak is investigated using an extensive set of diagnostics, permitting the instantaneous neutron yield, the radial profile of the neutron emission and neutron energy spectra to be studied. Apart from their importance as an immediate indication of plasma fusion performance, the customary use for neutron measurements is as a test of the internal consistency of the non-neutron diagnostic data, from which the expected neutron production can be predicted. However, because contours of equal neutron emissivity are not necessarily coincident with magnetic flux surfaces, a fully satisfactory numerical analysis requires the application of highly complex transport codes such as TRANSP. In this paper, a far simpler approach is adopted wherein the neutron emission spatial profiles are used to define the plasma geometry. A two-volume model is used, with a core volume that encompasses about 2/3 of the neutron emission and the peripheral volume the remainder. The overall approach provides an interpretation of the measured neutron data, for both deuterium and deuterium-tritium plasma discharges, that is as accurate as the basic non-nuclear plasma data warrant. The model includes the empirical assumption that particles, along with their energies and momenta, are transported macroscopically in accordance with classical conservation laws. This first-order estimate of cross-field transport (which, for deuterium-tritium plasmas, determines the d:t fuel concentration ratio in the plasma core), is fine-tuned to reproduce the experimental ion and electron temperature data. The success of this model demonstrates that the observed plasma rotation rates, temperatures and the resulting neutron emission can be broadly explained in terms of macroscopic transport.

1. INTRODUCTION

The neutron emission from an additionally-heated discharge in a tokamak is determined by the thermal properties of the bulk plasma and the super-thermal fast ion populations, of which the most important are deuterons and tritons, resulting from neutral beam injection (NBI) or ion-cyclotron range of frequencies heating (ICRF). In order to claim an understanding of the fusion performance of any discharge, it is necessary to be able to predict satisfactorily the resulting neutron emission on the basis of the measured properties of the plasma and of the heating techniques employed. As a rule, the detailed effects of the ICRF heating can only be modelled adequately with a specialist code, such as PION (Erickson *et al* 1993). Even with NBI heating alone, a complete treatment requires a complex transport code, such as TRANSP (Budny *et al* 1992), in which the particle effects can be modelled using Monte-Carlo techniques. Recent versions of TRANSP also include a RF-modelling package. The application of such codes is non-trivial and the computer processing time per discharge is considerable.

The work described in this paper represents an empirical attempt to model the neutron emission in the simplest possible manner, based mainly on classical conservation principles and a broad generalization concerning transport phenomena. The overall approach involves predicting the ion

and electron temperatures and, hence, the neutron emission on the basis of the measured plasma rotation rates and electron densities. An estimate of cross-field transport is implicit in this calculation. The temperature predictions can then be forced to reproduce closely the experimentally determined temperatures by suitable adjustment of two normalization constants; once this has been achieved, the cross-field particle transport is considered reliable. (Knowledge of the particle transport is necessary for determining the core plasma fuel mix for deuterium-tritium plasmas). Finally, either the refined predicted temperatures or the empirical temperatures may be used for comparison of calculated with empirical neutron emissions.

The NEPAM (Neutron Emission Prediction and Modelling) computer code is unique in that the plasma geometry for the central region, responsible for the bulk of the neutron emission, is derived from the neutron profile monitor in preference to the customary usage of magnetic flux surfaces. In part, this is advantageous because the neutron profile monitor permits the core geometry to be defined more precisely than is possible using magnetic measurements at the plasma boundary. It also avoids the need to take account of finite Larmor radius and neo-classical effects, which can cause the contours of neutron emission to depart appreciably from the flux surface prescription. An extreme example of this happening is discussed in Jarvis *et al* 1996, where the fusion product gamma-ray and neutron emissions are shown to be strongly displaced to the low field side of the magnetic axis during high power off-axis ICRF-heating experiments. A more commonplace example is that of neutral beam heated discharges, where the outermost neutron emission contours are found to depart appreciably from the magnetic surfaces in the region just above the magnetic divertor.

The neutron emission predicted with the simpler code is generally found to be in good agreement with that obtained from TRANSP using the same experimental data.

The present work is based on an earlier paper (Jarvis 1997) in which it was demonstrated, for a range of NBI-heated deuterium discharges, that it was possible to deduce satisfactorily the ion and electron temperatures through an iterative (and tedious) approach based on reproducing the measured neutron emissions from those regions. In both present and earlier models, the plasma was divided into core and peripheral regions with geometry defined from experimental neutron emission profile data rather than by computed magnetic flux surfaces. The observation that the earlier model also satisfactorily reproduced the plasma rotation rates (determined from charge-exchange spectrometric measurements) provided the incentive to test the possibility, now implemented, of using these measured rotation rates in an automatic iteration procedure. Thus, the neutron emission is now predicted rather than being included within the iteration scheme.

The code described here links together all the neutron diagnostic data available at JET, including deuterium-deuterium (d-d) and deuterium-tritium (d-t) neutron emission rates and radial profiles, and provides a necessary step in the calculations of neutron energy spectra for comparison with measured spectra. It utilizes much of the available diagnostic profile data for bulk and impurity ion species and for electrons and only requires flux surface information to define the position of the separatrix.

The material of the paper is presented in the following order. In section 2, the analysis of the

neutron profile data is described and typical findings are outlined. Section 3 describes the processing of non-neutron diagnostic data into a form suitable for use by the neutron prediction code. Section 4 contains a brief description of the neutron prediction code, which embodies a simple but nevertheless effective scheme for computing the cross-field transport of particles, momentum and energy. For d-t plasmas, this approach automatically provides the required estimate of the tritium concentration in the plasma core. Section 5 contains a discussion on the accuracy with which the neutron emission can be predicted from the measured non-neutron data. Section 6 concludes by applying the code to such varied topics as triton burnup studies, trace tritium transport experiments, alpha-particle-heating experiments during d-t discharges, the highest performance d-t discharges and to the interpretation of neutron energy spectra.

2. NEUTRON EMISSION PROFILES

The neutron profile monitor (fig.1) consists of two cameras, the smaller of which contains 9 collimated viewing channels in a fan-shaped array with a nearly vertical view through the plasma while the larger has 10 channels and a nearly horizontal viewing direction. The plasma coverage is adequate for neutron tomography, although the spatial resolution is coarse - neighbouring channels are 15 to 20 cm apart as they cross near the plasma centre. Two sets of neutron detectors are provided, so that d-d neutrons and d-t neutrons can be recorded separately. However, while it is easy to distinguish d-t neutrons from d-d neutrons, it is not possible to prevent the d-d neutron detection channel from responding to d-t neutrons. Thus, d-d neutrons can only be satisfactorily distinguished when the d-t neutron flux is less than a few times greater than the d-d neutron flux. Further details of the neutron profile monitor have been provided by Adams *et al* 1993 and Jarvis *et al* 1997.

In effect, the profile monitor contains 19 low-resolution neutron spectrometers, with quite complex signal processing electronics for the d-d neutron channels. The channels do not all have the same geometry and very extensive Monte Carlo neutron transport calculations are required to evaluate scattering and attenuation effects and so to establish the effective detection solid angles. Once this has been done, the profile monitor provides an independent, absolute, measure of the instantaneous neutron yield that agrees with measurements obtained from the neutron activation system (Jarvis *et al* 1991) to well within the estimated combined errors of about 15 %. Individual channels mostly exhibit relative efficiencies that fluctuate by ±10% for d-d plasmas and by ± 5% for d-t plasmas.

Because the channel-to-channel efficiency variations are non-negligible, a least squares fitting data analysis approach is used to smooth the neutron profile monitor data. A computer code (YAPAN) has been written that assumes a parametrized form for the radial neutron emissivity. The recorded signals are simulated by line-of-sight integration across the modelled plasma and the fitting parameters are optimized. Several constraints are applied: the emissivity profile should have smoothly-varying first and second derivatives, the instantaneous neutron yields derivable independently from the two cameras must be constrained to be identical and, optionally, may be

adjusted to reproduce exactly the instantaneous yield provided by a standard set of fission chambers. These chambers are, in turn, normalized to the activation measurements (Jarvis *et al* 1991). The fitting code will only provide satisfactory results when the quality of the input profile data is high. The fitting code itself, which has been developed over many years, must not contain too many adjustable parameters if the computer time is not to become excessive. The neutron emissivity contours are described using a system of nested ellipses having a common, but time-dependent, elongation. The centroid of the outermost ellipse is fixed at 30 cm. above the geometrical centre of the vacuum vessel. The centroid of the innermost surface is displaced relative to that of the outermost surface as required by the fitting program, with all other centroids interpolated linearly between these two extremes. The analysis generates neutron radial emissivity profiles with time bins of 50 ms and/or 500 ms and/or time-integrated over the whole shot, depending on neutron emission strength; 50 ms time binning is normal for JET processed data.

An important subsidiary result from the fitting code is the evaluation of the core volume, defined as the ratio of the total instantaneous neutron yield and the central neutron emissivity. This, of course, is the volume that would be occupied by the neutron-emitting portion of the plasma if the emission profile were to be flat and equal to the central emissivity. The actual fraction of the neutron yield emitted from the core volume is another useful quantity, which is typically about 2/3, regardless of profile peakedness. The core volume provides an immediate indication of plasma discharge type, as follows. The whole plasma volume of the JET tokamak is 80 m^3 with the pumped divertor installed. The core volume for a high-density, rather cold, high-confinement mode (ELMY H-mode) discharge can be as large as 40 m^3, that for a hot-ion H-mode discharge is typically 15 to 20 m^3, while for an optimized shear discharge it can be as low as 6 m^3. The core volume expands abruptly at each significant sawtooth crash, before shrinking rapidly back to the pre-crash value. A code that uses the core volume as an input parameter therefore has the possibility of automatically incorporating the essential consequences of sawtooth crashes and other important MHD disturbances. The use of a single time-dependent core volume gives results roughly equivalent to the use of a number of fixed volume elements.

A typical example of the use of the data obtained with the neutron profile monitor is illustrated in figs. 2 to 7. The selected discharge (# 50623) was run in deuterium, with good quality experimental data available. It is a medium density (fig. 2) ELMY H-mode discharge employing combined heating, 8 MW NBI and 4 MW ICRH, and exhibiting 2 Hz sawtooth oscillations. The effective charge (Zeff) is rather high (about 3) and the neutron yield reaches 4×10^{15} n/s. A 3-D plot of the line-integrated measurements from the neutron profile monitor is presented in fig. 3. This combines data from both cameras in a single plot, channels 1 through 10 corresponding to the horizontal camera and 11 through 19 to the vertical camera. The time binning is 50 ms and the data have been smoothed with the YAPAN fitting code. The profile is strongly peaked, due to the RF-heating, with the vertical-viewing camera profile having higher peak values because of the plasma vertical elongation. Rather more detail can be seen in fig. 4, which presents the same data in contour form.

In order to emphasize changes in profile shape rather than of neutron intensity, the profiles have been normalized to constant neutron emission strength. The profile maintains the same general shape for the entire beam-heating period, with the intermittent occurrence of the sawtooth crashes superimposed. Fig. 5 shows the performance of the fitting code for a single time bin. Two signals are shown: "MODS" are the fully corrected line-integrated data summed over the chosen time-interval and normalized so that the integrated yields from the two cameras correspond precisely with the yield provided by the fission chambers, while "FITS" are reconstructions derived from the results of the fitting code. The two normalization factors usually differ from unity by less than 10%. The slightly lower peak amplitudes exhibited by "FITS" in fig. 5 could be a consequence of form of parameterization adopted for the neutron emissivity profile, which has difficulty in reproducing exceptionally strongly peaked profiles, although the "MODS"/"FITS" ratios for all channels usually exhibit ±10% scatter for d-d plasmas. The plot shown corresponds to 7.0 s, when the emissivity peaking was at its strongest. The derived emissivity profile at this time is shown in fig. 6. Finally, two of the key quantities derived from the profile data that will be used throughout the remainder of this paper are shown in fig. 7; these are the effective core volume (obtained by dividing the total neutron emission strength by the peak neutron emissivity) and the corresponding fraction of the neutron emission originating from the core volume. The plasma elongation of 1.35 (radially invariant, as derived from YAPAN) changed little throughout the discharge. It should be remarked that the flux surface elongations vary with minor radius, rising from about 1.3 near the magnetic axis to about 1.8 near the separatrix. Fig. 7 shows the sudden expansion and recovery of the plasma volume during sawtooth crashes and shows the core volume for discharge 50623 to be 10 m^3 or less, a consequence of the central ICRF heating.

3. PREPARATION OF DIAGNOSTIC DATA

As the neutron emission is strongly concentrated near the centre of the plasma, it is not unreasonable to represent it by a two-volume model. The fitting programme YAPAN provides the position, elongation and volume for the core region and the position and elongation (the same as for the core, by default) for the peripheral region. However, the volume adopted for the peripheral region is that defined by the magnetics code EFIT (O'Brien *et al* 1992) in order to preserve the overall particle inventory. A FORTRAN pre-processor code (PLASMATH) is used to prepare two sets of plasma parameters (core and periphery) that are appropriately volume-averaged. To perform this operation, each of the two regions is subdivided into a number of nested ellipses so that appropriately averaged densities, temperatures, Zeff values, etc. can be prepared using the measured full radial profiles for these quantities. These averages over core and peripheral volumes are then adequate for use in the two-volume model, without noticeable loss in accuracy for most purposes. In particular, they are suitable for calculating the beam-plasma neutron emission as this scales only somewhat less than linearly with ion and electron temperatures. The exception is for the thermal neutron emission, which varies with ion temperature as Ti^{α}, with power dependence α ranging from above 5 (below

Ti = 1 keV) to 2 or lower (above 10 keV). Therefore, the thermal neutron emissions for core and peripheral volumes are also computed using the multi-volume approach and core and peripheral "neutron" temperatures are derived that conserve the thermal neutron yields. The ratios of the two sets of ion temperatures ("neutron" and bulk average) are then used in the NEPAM code to correct the computed average temperatures for profile effects, but only when calculating the thermal neutron emission. This refinement is unnecessary for the core volume, for reasons related to geometry, and is relatively unimportant for the peripheral volume because the peripheral thermal neutron yield is generally smaller than the beam-plasma yield. However, it is important to perform the (peripheral) calculation as accurately as possible when the thermal neutron yields are to be compared with results derived from other computer codes, since precise agreement should be obtained when the same input data are utilized.

The core volume is easy to adjust in position, shape and volume for the purpose of performing sensitivity calculations. In this way, we find that a 10-cm radial shift of the core volume results in a 30% change in the predicted neutron yield for a typical hot-ion H-mode discharge. The relevance of this arises from the uncertainty of between 5 and 10 cm in the radial position of the magnetic axis as determined from magnetic measurements. Changes to the core region elongation lead to relatively smaller changes in predicted neutron yield. The precise definition of the core volume has no effect on the calculated thermal neutron yield, and very little on the beam-plasma yield. A reasonable choice must be made, however, if the neutron emission profile is to be reconstructed realistically.

At JET, electron densities and temperatures are measured with two different diagnostics. The present code uses the processed data provided as part of the analysis process for the Charge Exchange Recombination Spectroscopy (CXRS) diagnostic (Mandl *et al* 1993 and von Hellermann *et al* 1996a). The LIDAR (Gowers 1991) electron density measurements are adopted for the density radial profiles, normalized to the line-integrated data from the interferometer measurements (Veron 1982); radial and temporal smoothing and interpolation is performed. Electron temperature measurements from LIDAR (Gowers 1991) and ECE (Costley 1991) measurements are available. LIDAR electron temperatures, suitably smoothed and interpolated are generally used by the CXRS analysis code, CHEAP (von Hellermann *et al* 1996b), and by TRANSP. The two sets of temperature profiles usually agree within experimental errors, with the ECE results tending to be somewhat higher. For high-density discharges run with low toroidal magnetic field, the ECE measurement predictably fails because the plasma is no longer transparent to the second harmonic radiation, leading to very low ECE temperatures.

4. THE NEUTRON PREDICTION CODE

The prediction code NEPAM is written in Mathcad Plus 6.0 *. A few approximations are made for computational simplicity. The minor errors so introduced are not considered significant in relation to the existing uncertainties in the experimental data. The main approximation is to the geometry of the neutral beam injectors; the beam-lines are all assumed to lie in the plasma mid-plane instead of

subtending a range of small angles to it, which should be acceptable provided the core volume does not become unduly small (i.e. less than 6 m^3). Other approximations are implicit in the adoption of a two-volume model. For example, slowing down beam-injected ions are assumed to be retained within, but distributed uniformly over, the volume into which they are deposited.

The basic physics concepts incorporated in the code may be found in textbooks (e.g. Wesson 1997). The fast particle slowing down formalism is the Stix simplification (Stix 1972) of the Spitzer formulation (Spitzer 1962), in which the rate of loss of energy, E, is written

$$\frac{dE}{dt} = -\frac{\alpha}{\sqrt{E}} - \beta E$$

Beam-plasma and beam-beam fusion reaction rates are computed following the prescription of Core and Zastrow 1996. Angular momentum deposition by beam injection has been studied experimentally by Zastrow et al 1998. Hinton and Rosenbluth 1999 cover the theoretical demonstration that beam ions injected into trapped orbits transfer their angular momentum directly and locally to the plasma. This is a troublesome concept, most easily understood on the basis that ions entering trapped orbits create a radial electric current that must be self-cancelled in a highly conducting fluid, i.e. a plasma current (carried by thermal ions) flows to cancel it out. This current flow gives rise to exactly that $\mathbf{E}\times\mathbf{B}$ force required to transfer the momentum from the beam ions to the plasma. This transfer is effectively instantaneous.

NEPAM offers two modes of operation for those sections of the code that precede the calculation of the neutron emission. The simpler mode serves as a test of the self-consistency of the available diagnostic data with the neutron data. This mode is useful for deuterium plasmas but often proves unsatisfactory for deuterium-tritium plasmas, since it assumes no cross-field transport between core and peripheral regions. Instead, it assumes that the deuterium to tritium concentration ratio in the core is the same as at the plasma edge. Only edge measurements of this ratio are available, and then only for concentrations in excess of 5%. There are just the two plasma volumes to consider, for which suitably averaged quantities have been prepared as described in the previous section. The thermal ion densities are inferred from the electron densities and the CXRS-derived Zeff values and impurity identifications, corrected for the fast ion contents due to the neutral beams and from ICRF-heating. The ion and electron temperatures are the volume-averages of the experimental measurements. This mode of operation consists of little more than preparation of volume-averaged experimental data (using PLASMATH), assessment of the neutral beam deposition in the plasma and the calculation of the neutron emission as described at the end of the present section.

The second mode of operation for NEPAM involves an empirical model of the cross-field particle, energy and momentum transport between core and peripheral volumes, including the neutral influx and losses between peripheral volume and the vessel walls. To perform such a calculation rigorously would be a major challenge. Fortunately, a rather simple implementation proves adequate - at least, for our immediate purpose of interpreting the neutron emission. We start with a trivial observation: for a hypothetical plasma that exhibits effectively instantaneous cross-field transport

the density and temperature profiles would be flat across the whole volume, apart from an abrupt boundary region. The change in axial properties after injecting a known number of neutral particles into such a plasma is trivially calculated, since the instantaneous cross-field transport ensures the introduced particles, along with their physical attributes, are distributed uniformly across the entire plasma. Since cross-field transport in real plasmas is indeed rapid, we should not be too surprised if a simple scheme derived from the preceding observation happened to work rather well in practice, especially when the plasma volume is broken up into two (or more) regions.

The neutral particle flux entering the plasma is given by the product of Johnson-Hinnov factor (Johnson and Hinnov 1973) and the calibrated signal from the measurements of the Hα radiation intensity, assuming this latter local measurement to be representative of the whole plasma. The Johnson-Hinnov factor, giving the number of neutrals per observed Hα photon, varies from about 5 to 30, depending on edge conditions in a manner that we will not examine here. As our geometrical model involves core and a peripheral region, we introduce a pseudo Johnson-Hinnov factor to describe the particle flow from the peripheral region into the core, while expressing that influx in terms of the recycling flow of neutrals into the peripheral volume. This provides two "Johnson-Hinnov" factors to be adjusted (JH_c for the core region and JH_p for the peripheral region) and permits the core particle influx to be assessed on a similar basis as the recycling influx into the peripheral volume. This accounts for the gas fuelling of the plasma. The particle losses from the two regions are expressed through two particle confinement times, τ_c and τ_p. These four parameters, the Johnson-Hinnov factors and the confinement times, are optimised as described below.

Plasma rotation rate data are recorded by charge-exchange spectroscopy while neutral beam heating is being employed. It is assumed that the momentum carried in by the beams is deposited locally, even when the beam ions enter trapped particle orbits (Hinton and Rosenbluth 1999). It is further assumed that the only input torque acting on the plasma is that derived from the neutral beams and that the only external drag is that provided by the influx of recycling neutral particles. Neutral beam deposition fuels both core and peripheral volumes. In addition, the plasma core is fuelled from and exhausts to the peripheral volume while the peripheral volume simultaneously reacts to the demands from the core but otherwise fuels from and exhausts to the vessel walls. Thus, the core is accelerated by the beams and has to be slowed down by fuelling from the peripheral volume. Since this will result in the core being over-dense, the core electron density has to be lowered to match the measured value. JH_c controls the fuelling of the core from the periphery; τ_c controls the particle exhaust to the periphery. Simultaneously, plasma properties of the peripheral volume are made to reproduce its measured rotation rate and density values; the particle transfers with the core have already been determined and neutral influx from and losses to the walls have to be included. Provided the relative densities of the ion species (including tritium and deuterium) in the periphery are known, their relative densities in the core will be determined by the calculation. The transport scheme is macroscopic in that it involves bulk plasma properties. The impurity content in the periphery has to be adjusted to reproduce the measured Zeff value, since there are no direct

measurements of the carbon influx. The core Zeff as directly computed generally agrees with the measured data within the experimental errors. Alternatively, the measured core Zeff values can be imposed.

In summary, an automatic iteration routine is employed to oblige the modelled plasma to track the measured rotation rates, electron densities and Zeff data. The routine generates the two pairs of intermediate entities, i.e. the two factors JH_c and JH_p, and the effective particle confinement times τ_c and τ_p, for core and periphery, respectively. In passing, we note that JH_c and JH_p are found to be approximately equal (in the range 5 to 30) for ELMy H-mode discharges, but that JH_c diminishes relative to JH_p as the plasma confinement properties improve. This rotation rate and density tracking calculation is explained more fully in the Appendix.

After the momentum and density tracking calculation has been performed, energy conservation is used to establish the ion and electron temperature evolutions. It is now essential to distinguish between slowing down fast ions and the thermal ions. The heating calculation is straightforward, but extensive; some details are provided in the Appendix. It would be surprising if it were found possible to calculate the experimental ion and electron temperature data accurately on the basis of the above over-simplified model, if only because the basic experimental data have non-negligible associated experimental uncertainties. However, a satisfactory reproduction of the measured temperature data is readily obtained by introducing (somewhat arbitrarily) just two normalization constants for a given discharge, $Frot_c$ for the core and $Frot_p$ for the periphery. These are used as multipliers of the beam momentum deposition terms. These two multipliers might be expected to be time-dependent, but simple constants have been found acceptable in practice. Their values are found to change with quality of the discharge, from 0.7 to 1.1 for $Frot_c$ in the core and from 0.7 to 0.3 for $Frot_p$ in the periphery, covering the range from hot-ion H-mode to ELMY H-mode plasmas. The core values could be considered consistent with the expected value of unity if a systematic uncertainty of about 20% is attributed to experimental errors. More probably, the core volume discrepancy is real and is associated with the use of only two regions, resulting in excessive averaging. Indeed, it may well be the case that the relative success of the calculation is related to the empirical observation that the radial profiles of rotation rate and ion temperature are rather similar. The peripheral values appear to be more discrepant, but it should be appreciated that the multiplier affects only the torque introduced by the beams deposited directly in the peripheral region and does not act on the approximately equal torque due to particle flow out of the core. We should, however, expect the multiplier to be smaller than unity as the calculation takes no account of electromagnetic braking effects, as exemplified by locked-MHD modes as the extreme case.

A first estimate of the normalization constant for the periphery, $Frot_p$, can be obtained prior to running the temperature calculation. A few iterations of the momentum-transfer routine yields a value for $Frot_p$ that generates a peripheral particle confinement time τ_p behaviour that satisfies the global energy balance requirement (energy input versus energy content plus loss) throughout the discharge using measured temperature data. ($Frot_p$ modifies the torque applied to the peripheral

region; this determines the neutral influx "drag" required to reproduce the measured rotation rate and, hence, affects τ_p because the electron density has also to be reproduced). Requiring the calculated and measured core and peripheral temperatures to agree then produces optimized values for $Frot_c$ and $Frot_p$. It should be emphasized that – in the absence of ICRF heating – the code unambiguously determines the core and peripheral region ratios of T_i to T_e for each time-step. Thus, electron temperature data alone suffice, should ion temperatures not be available.

This temperature calculation for the periphery assumes that the energies carried off by lost ions and electrons are those typical of the bulk peripheral plasma, whereas it might be thought that lower energies might be appropriate since neutral formation, transport and losses must be important near the plasma edge. Interestingly, because a satisfactory global energy balance is demanded, it is found that the calculated temperatures can only be made to agree well with the measured temperatures when energies close to the bulk peripheral values are used, which essentially removes this further degree of complexity. While the need for the normalization constants $Frot_c$ and $Frot_p$ is a little disappointing, the achievement of satisfactorily reproducing the measured ion and electron temperatures, and more particularly their empirical ratios, provides a measure of confidence in the underlying particle transport and in the computed core tritium/deuterium density ratios.

Temperature calculations can also be performed for ICRF-only and for combined NBI + ICRF heating. However, the effect of ICRF heating on the plasma is not as straightforward as for NBI as no attempt has been made to treat the RF wave problem correctly. However, major simplifications are possible, as the main consideration is that of energy conservation. For example, when the RF heats the bulk plasma indirectly through the production of a fast ion tail, perhaps extending up MeV energies, we can expect the heating to be shared approximately equally between core and periphery because of the large banana widths of the fast ions (the fast ion orbits cross into the periphery). The heating power then goes mostly into electrons. This situation is readily modelled provided the ICRF power deposition is modest (a few MW only). The generation of significant neutron yields from accelerated deuterons and tritons interacting with thermal deuterons and tritons, or of protons and ^{3}He ions interacting with impurity ion species, lies outside the scope of the present paper.

Apart from the use of calculated or measured temperature data, the neutron emission calculation is the same for both modes of operation. The thermal neutron emission calculation is straightforward, using the fusion reactivity formulation of Bosch and Hale 1992. The beam-plasma neutron production is computed in two ways, depending on the fast ion slowing down times relative to the chosen size for the time bins. When the slowing down time is relatively long, a multiple energy group slowing down formalism is used. Otherwise, a steady-state calculation is needed. In either case, hot-ion reaction cross-sections are used, as described by Core and Zastrow 1996. A small correction for beam energy enhancement due to thermal up-scatter is included (e.g. adding 3/2 T_e in recognition of the electron-ion, but not the ion-ion, equilibration time being much shorter than the ion slowing down time). Beam-beam calculations are performed (Core and Zastrow 1996) in the multi-group

approximation but relying on TRANSP for normalization purposes since the exact calculation demands a multi-volume approach and an accurate geometry for the neutral beam injectors. Beam-beam neutron emission is generally comparatively small. A triton burnup calculation is performed, assuming the tritons remain within the regions in which they are born (hence, no orbit losses). Similarly, alpha-particle production is taken into account, including heating effects. Finally, a very approximate model of ICRF-accelerated deuterons or tritons is included for investigating those RF-heated discharges for which the measured neutron emission appreciably exceeds that which can be attributed to thermal plus beam-induced emission. The scheme adopted involves using the deposited ICRF energy to promote thermal ions of species appropriate to the applied radio frequency to a representative single energy and then permitting them to slow down as if impervious to the influence of the RF waves, thereby simulating an effective fast-ion tail temperature. This procedure works satisfactorily for discharges exhibiting relatively frequent sawtooth crashes, but fails conspicuously when the intervals between giant sawteeth have periods in excess of one second. The generally preferred ICRF heating scheme involves tuning to minority ion species such as hydrogen or ^{3}He ions (for which the RF-accelerated ions should not directly undergo neutron-emitting fusion reactions) in such a manner that RF energy is efficiently transferred to the thermal plasma. One such example is illustrated in fig. 8, for the deuterium discharge # 50623. The agreement between the total computed 2.5 MeV neutron yield and the measured yield is entirely acceptable. The separate contributions from beam-plasma and thermal neutron emission are shown (the beam-beam contribution is negligible). For this discharge, the ICRF heating was tuned to protons and there is no indication of second-harmonic acceleration of deuterons. For completeness, it should be pointed out that strong ICRF populations of energetic protons or ^{3}He ions are indeed capable of generating significant neutron emission through interactions with impurity ions such as ^{9}Be and ^{12}C but this generally requires applied RF power levels in excess of 7 MW.

5. ACCURACY OF THE NEUTRON YIELD PREDICTIONS

There are two general sources of uncertainty when predicting the neutron yield from basic plasma properties, those of computational origin and those due to measurement imprecision. Computational uncertainty is generally ignored but can be appreciable. It includes numerical approximations (made for convenience) and simplifications (or even omissions) of complex physical phenomena. The combined significance of these computational uncertainties is best examined by comparison with a fully comprehensive code. For JET discharges, the most detailed code used is TRANSP, which includes most known phenomena and which makes heavy use of Monte Carlo techniques; it is computationally intensive.

The NEPAM code relies heavily on the diagnostic measurements obtained from the charge-exchange recombination spectroscopy (CXRS) diagnostic (Mandl *et al* 1993). The CXRS associated code CHEAP (von Hellermann *et al* 1996b) also predicts the neutron yield and is run for a significant fraction of JET discharges. It computes only thermal and beam-plasma neutron yields, for which a

steady-state beam-plasma calculation is performed and fast ions are assumed to remain on the flux surfaces on which they were created. CHEAP lacks a cross-field transport model and is only able to reproduce the measured d-t neutron yields when the d:t fuel mix has a flat radial profile.

The basic plasma quantities are subject to substantial experimental uncertainties. Table I provides estimates of their magnitude. The optical diagnostics suffer from various problems that are not included in the Table; e.g. windows become coated with carbon, which reduces their optical transmission properties in a manner for which compensation may not be possible. Furthermore, many optical devices have a real potential for becoming misaligned, which may result in radial profile mapping errors. Using the data in the Table, the absolute uncertainty (total error obtained by summing in quadrature) for a d-d plasma giving equal beam-plasma and thermal neutron production contributions is found to be approximately ± 25% for a good quality plasma with Zeff ~ 2. Close agreement between prediction and measurement (i.e. well within the 25% uncertainty) is therefore likely to be purely fortuitous. Of course, since Zeff is often large, there is a natural tendency to adjust its normalization (within its stated experimental uncertainties) until a good fit between prediction and measurement is obtained. Doing this transfers uncertainties from other measurements to Zeff.

Table I

Estimated accuracy of measured quantities needed in the modelling of the neutron emission from JET discharges.

Quantity	**Accuracy**
Major radius of core centre (m)	± 0.04 m, from neutron profile monitor
Height of core centre above mid-plane (m)	± 0.04 m, from neutron profile monitor
Effective core elongation	± 0.2, from neutron profile monitor
Ion temperature overall scale factor:	
CXRS	± 5 - 10%
Plasma rotation rate:	
CXRS	± 5 - 10%
Electron temperature overall scale factors:	
LIDAR	± 10%
ECE	± 10%
Electron density overall scale factors:	
LIDAR	± 7%
Interferometer	± 1% line-integrated
Zeff overall scale factors:	
Visible bremsstrahlung	± 50%
CXRS	± 20%
Major impurity species and concentrations	± 20%
Tritium/Deuterium conc. ratio in plasma	Not directly measured
Neutral Beam Powers	± 10% all *PINIs together, ± 15% each individual *PINI.
Neutron yield calibration	± 10%

*PINI - Positive Ion Neutral Source.

The reliability of the performance of NEPAM (using empirical temperature data) in predicting the neutron yield has been assessed through comparisons with TRANSP. A satisfactory comparison of NEPAM and TRANSP thermal and beam-plasma neutron yield predictions was carried out previously (Jarvis 1997) for a series of hot-ion H-mode discharges. Subsequently, numerous comparisons have been made for a variety of discharge types, including a low temperature ELMY H-mode discharge (with beam-plasma emission totally dominant) for which the results were essentially identical.

The final test of NEPAM is the comparison of predicted with experimental yields. From a range of assorted d-d discharges, it is found that it over-estimates on average by about 5% but with much scatter. Given all the uncertainties in the raw data, this is a very satisfactory result. However, there is scope for improvement in the code. For example, it ignores the cross-field diffusion of slowing down beam ions; taking this into account could alter the initial co-counter streaming ratio and, hence, would raise somewhat the beam-plasma neutron emission. While this is not an important effect in determining the neutron yield, it is amenable to investigation through careful examination of neutron energy spectra measured along a tangential line-of-sight, as will be discussed later.

6. FURTHER TESTS OF THE CODE

The code has been successfully applied to a wide variety of discharges, with no major problems being encountered except in those instances where important physics is completely omitted (high-power ICRF heating in which light ions are accelerated strongly and undergo neutron-emitting nuclear reactions with impurity ions, and deep fuelling with deuterium pellets). The following examples all involve d-t discharges as these most clearly exploit (and test) the empirical transport model. Section 6.1 provides an example of a triton burnup measurement, for which the transport model is invoked to substitute missing ion temperature and rotation rate data. Section 6.2 demonstrates the deduction of tritium concentration in a plasma using deuterium neutral beam blips; again, the transport model is required to substitute missing data before and after the beam blip. Section 6.3 describes trace-tritium gas puffing experiments; it is shown that the model adequately describes the transport of tritium between the plasma edge and the core. Section 6.4 describes the performance of the best discharge in the alpha-particle heating experiment. Section 6.5 concerns the record fusion power d-t discharge, which included modest RF power heating. Section 6.6 shows that the model can be applied to an optimised heating discharge in deuterium, despite the use of high power RF heating. Finally, section 6.7 describes the prediction of neutron energy spectra from d-t discharges; the spectra provide a further test of the d:t fuel concentration ratios calculated by the model. The examples presented in this section are typical in the sense of code performance but otherwise are mostly discharges chosen for their importance for the JET research programme.

6.1 TRITON BURNUP

One branch of the d-d fusion reaction releases a 1.0 MeV triton (τ). The τ-d fusion cross-section

exhibits a strong maximum at about 200 keV energy for the slowing down tritons. Hence, the associated 14-MeV neutron emission is delayed relative to the 2.5-MeV neutron emission by the time taken to slow down from 1000 to 200 keV, which is typically a few hundred milliseconds for high-performance JET discharges. Since the burnup triton has a gyro-radius similar to that of a fusion alpha particle, the study of its confinement properties provides a method of studying alpha particle behaviour without operating the tokamak with d-t plasmas. There are experimental difficulties, however. Firstly, the burnup probability is typically of order of 1 - 2% only, so it is necessary to measure a weak 14-MeV neutron signal in the presence of a two-orders of magnitude greater 2.5-MeV neutron "background". Secondly, once tritium gas has been introduced into the tokamak, as was done during the DTE1 experiment at JET, then the residual tritium outgassing from the walls thereafter provides a competing 14-MeV neutron signal.

For JET, when operated with plasma current/toroidal magnetic field conditions in excess of 2.5 MA, 2.5T, the fast tritons are expected to be fully confined. Moreover, due to the high plasma currents and large plasma volumes, it is reasonable to assume that the triton orbits remain close to the flux surfaces on which they were born. Neutron profile measurements have shown that this is indeed the case. The triton burnup calculation is then straightforward. The NEPAM predictions have previously been shown (Jarvis 1997) to be in good agreement with the experimental measurements for hot-ion H-mode conditions. We examine here the burnup for a 3.0 MA, 3.5 T discharge # 49755, heated with 15 MW NBI. This high performance discharge exhibits a peak 2.5 MeV neutron yield of 2×10^{16} $n.s^{-1}$. As there are no CXRS ion temperature and rotation data for this discharge, it was necessary to compute these quantities; the predicted and measured 2.5 MeV neutron yields are in fair agreement. The computed triton burnup signal is reasonably immune to any uncertainties so introduced, since the measured 2.5 MeV signal is used as a source of tritons and the τ-d neutron production depends mainly on the electron temperature, for which good measurements were available. The calculations and measurements are compared in fig. 9, where the customary delay between 2.5 and 14 MeV neutrons of about 0.8 s for high temperature discharges is displayed. The initial rate-of-rise of the measured 14 MeV neutron signal is indicative of a residual low level of tritium in the plasma (approx. 30-ppm). The agreement between calculation and measurement demonstrates the reliability of the beam particle slowing-down and fusion reaction rate calculations.

6.2 TRITIUM CONCENTRATION DETERMINATIONS

One of the first investigations carried out in the JET d-t experiment involved fuelling the plasma with different mixtures of deuterium and tritium in order to vary the plasma concentration from pure deuterium to pure tritium. A number of techniques were used for determining the tritium concentration. One of these involved measuring the neutron emission strength from a single brief burst of deuterium beam injection, from which the tritium concentration was calculated using the NEPAM code. Several bursts of the deuterium beams were used during each discharge so that the time evolution of the tritium concentration in the plasma could be studied following a prior period of tritium gas injection.

The calculation entails establishing the tritium content by adjusting the assumed concentration until the predicted and measured neutron yields agree at the moment of peak yield during the beam-blip. Naturally, the same concentration is also required to reproduce the neutron emission during the ohmic phases of the discharge. As there were no measurements of ion temperature or rotation rate available, it was necessary to compute the ion temperatures, with a constraint that the calculation must reproduce the measured electron temperatures. The JH_c and JH_p factors were treated as constants to be manually adjusted to achieve this, in contrast with the usual situation where rotation rate measurements are available when they become automatically calculated time-dependent quantities. (Without rotation rate data, the $Frot_c$ and $Frot_p$ parameters are redundant). The resulting tritium concentration was determined to about 20% accuracy only, with the beam powers providing the major element of uncertainty (see Table I). A comparison of different techniques for measuring the tritium content showed (Jarvis et al 1998) that the tritium concentration at the edge was greater than in the centre at times early in the discharge (as for fig.10) but that the concentration had become uniform when measured 5 seconds later.

The temporal dependence of the neutron emission during and after the beam blip offers an excellent test of the beam ion slowing down calculation as implemented in the code. This is shown in fig 10, where a logarithmic plot is used to display the relationship between prediction and measurement; the small discrepancy that can be seen is well within the uncertainties of the basic plasma data, primarily of electron density and temperature.

The 14-MeV (t-d) neutron emission profile at 17.12 s, measured during the neutron yield flat-top of the beam-blip, is found to be adequately reproduced by the prediction from the two-volume model, see fig. 11. Note that the NEPAM calculation should be compared with the fitted profile, rather than the directly measured profile that has been neither normalized nor smoothed.

6.3 TRACE-TRITIUM DIFFUSION EXPERIMENTS

An excellent test of the ability of the model to simulate cross-field particle transport is found in the study of the trace-tritium gas-puffing experiments that were carried out early in the DTE1 experiment, before the vessel walls had become significantly loaded with tritium. The discharge selected as an example, # 42531, is one of a series of Greenwald density limit discharges (Greenwald *et al* 1988). The plasma current and toroidal field were 2 MA, 2T and the central electron density was 7×10^{19} m^{-3}. Strong deuterium gas fuelling was applied throughout, with a brief (nominally 60 ms) puff of tritium gas in the middle of the beam-heating period (6 MW of deuterium beams at 76 keV and a further 4 MW at 135 keV). The discharge was characterized by the strong ELM activity and nearly flat density profiles that are typical of H-mode discharges. The global neutron emission for this discharge is shown in fig. 12. (For clarity, the measured 2.5 MeV neutron emission is not shown; the calculated 2.5 MeV emission was carefully adjusted so as to reproduce the measured emission, as described below).

For initial analysis purposes, the discharge was assumed not to contain any tritium. The total 2.5-MeV neutron emission strength was obtained from the profile monitor, which permits the 14-

MeV and 2.5-MeV neutrons to be distinguished when the 14-MeV emission is not dominant. In this discharge, the ECE electron temperature data became predictably unreliable once the plasma temperature had fallen off from its initial maximum and the plasma conditions had become such that the escape of second-harmonic cyclotron radiation was inhibited. The LIDAR temperatures, of course, are not affected in this way. With no data adjustment, the plasma rotation was computed and the global energy balance tested using the measured ion and electron temperatures. $Frot_c$ was left at unity and $Frot_p$ was adjusted until an acceptable energy balance was achieved. The temperature calculation was then performed (with no further adjustment of $Frot_c$ and $Frot_p$) leading to an over-estimate compared with the CXRS ion temperature data (fig. 13) but providing very good agreement with the LIDAR electron temperature data (fig. 14). It may be noted that in cold, dense plasmas the CXRS ion temperatures are frequently measured to be lower than the electron temperatures, although this is a physically impossible result when the ion-electron equilibration is strong, as in this discharge. The global energy balance obtained with the calculated temperatures was excellent. The global particle confinement time was found to be 160 ms. Proceeding with the 2.5-MeV neutron emission calculation, predominantly beam-plasma in character, good agreement with the measured emission was found, permitting attention to be transferred to a study of the 14-MeV neutron emission.

The tritium level in the recycling gas was too small to be measured by the available edge and sub-divertor diagnostics. Consequently, it was necessary to deduce the tritium influx due to gas puffing and wall recycling from the study of the global 14-MeV neutron emission. Before the tritium gas puff, the tritium content of the recycling fuel was found to be 0.3%. The puff duration was assumed to be a step of 120 ms duration, with its magnitude chosen to reproduce the peak emission rate for the 14-MeV neutrons. As the calculated rate of decay of the 14-MeV emission after the gas puff was faster than observed, it was concluded that the tritium wall loading after the puff was somewhat greater than before. Adjusting the recycling level to be initially 1.3%, but decaying to 0.5% at the end of the measurement period with a 1.0 s time-constant, permitted the global 14-MeV neutron emission to be well-simulated during the period following the tritium gas injection. (The tritium puff duration adopted is double the opening period of the gas-valve but may more accurately represent the dispersion and transit time into the plasma. The precise duration assumed was not critical).

The analysis described above ensured that the calculated *global* 2.5-MeV and 14-MeV neutron emissions reproduced the measured *global* emissions. The key test of the 14-MeV neutron emission calculation is the comparison of the line-integrals calculated (with no further tuning) for the line-of-sight geometry of the neutron profile monitor with the actual measurements. It may be noted that the 2.5-MeV neutron line-integrals are essentially unaffected by the tritium gas puff. As the plasma model uses just two volumes, only an approximate level of agreement would be anticipated. In practice, the calculated and measured 14-MeV neutron line-integral data agree remarkably well. The agreement is very good for those channels that cross the plasma core, but less so for those with a view only of the peripheral region. Fig. 15 compares the calculated and measured data for the two

channels (one for each camera) that cross the plasma near the centre and one for a channel close to the plasma edge. The pairs of curves are normalized at their peak values for the purposes of this comparison. For the central channels, both the rise and fall of the neutron emission are evidently well simulated. For the edge channel, the calculated rise is faster than the measured rise but the after-puff behaviour is nevertheless adequately modelled. (The minor systematic fluctuation that may be seen in fig. 15 result from the present calculation being run using 10-ms time bins, introducing the need for interpolation between data-points stored at 50-ms intervals, as is customary for JET processed data). This high degree of agreement of calculation and measurement strongly supports the practical usefulness of the simple model of cross-field particle transport as employed in the NEPAM code, at least for ELMY H-mode discharges.

A rough estimate of diffusion coefficients can be made from the rate of decay of the calculated tritium levels in the core and peripheral volumes after the puff. The time-dependencies are shown in fig. 16. Using the relationship $D \sim a^2/5.6\ \tau_d$, where a is either the core minor radius or the width of the peripheral region, and τ_d is the exponential decay time of the tritium level, then we obtain $D \sim 0.12\ m^2/s$ for the core and $\sim 0.30\ m^2/s$ for the periphery. To avoid the influences of recycling, these decay times were obtained after re-running the calculation with cross-boundary tritium fuelling and post-puff recycling set to zero. For discharge # 42511, with comparable current, field, and electron density but with 70% higher electron temperature and 70% extra beam-heating power being applied (and no deuterium gas bleed) the deduced diffusion coefficients are $D \sim 0.20\ m^2/s$ for the core and $\sim 0.70\ m^2/s$ for the periphery. Uncertainties of at least ± 20% should be associated with these estimates. As the core densities are the same, we expect the (outwardly directed) core cross-field particle transport to be higher in the higher beam power case, as indeed observed. Trace tritium transport was examined in considerable detail in refs (Matthews *et al* 1999 and JET Team 1999) using a 1_-D transport code with diffusive and convective particle transport terms. The diffusion coefficients found in the earlier work for zones 0 and 1 are 0.14 and 0.37 m^2/s, respectively, for discharge # 42531 and 0.17 and 0.70 m^2/s for # 42511 (~10% error bars). If we associate zones 0 and 1 with the core and periphery of the present work, on the grounds that zones 2 and 3 lie at large radii from which the neutron emission is very weak, then the two sets of results appear to be fully consistent. If, however, we attempt to average the four-zone diffusion coefficients as appropriate to the core and peripheral region boundaries, then averaged values of approximately 0.3 and 1.5 m^2/s are deduced for both discharges, in apparent contradiction with the NEPAM calculations. However, the detailed study (Matthews *et al* 1999) analyzed the inward tritium diffusion during the gas puff, which would have appreciably perturbed the transport in the outer regions, whereas the NEPAM analysis examined the outward diffusion during the unperturbed post-puff phase. Consequently, only the core values should be compared.

One problem highlighted by CHEAP predictions of the neutron emission profiles is worth mentioning at this point, as it was a particular concern for the trace-tritium discharges. It is found that the measured line-integrated neutron emissions for channels 10, 9 and - to a lesser extent - 8 of

the neutron profile monitor are often much lower than predicted by the CHEAP calculations. One reason for this disagreement could be the assumption that fast ions travel around flux surfaces, whereas full orbit calculations demonstrate that beam ions initially deposited near the magnetic separatrix enter trapped orbits with turning points above the X-point region, with many of these ions subsequently leaving the plasma. TRANSP follows the full ion orbits and tends to obtain acceptable agreement with the experimental line integrals (however, TRANSP has not been applied to the trace-tritium discharges of present interest). An additional consideration (not modelled by TRANSP) is the apparent presence of a high-density cloud of neutrals located in the region of the X-point, above the divertor. The presence of such a cloud would necessarily lead to an enhanced loss of fast beam ions through charge exchange processes, since the turning points of trapped beam particles lie within the cloud. Although the peripheral profile measurements would be seriously affected, the total neutron yield would not be reduced significantly. This problem is avoided when analyzing the experimental neutron profile using YAPAN because this code does not use flux surfaces to define the plasma boundaries; instead, it assumes elliptical surfaces for which the common elongation is derived from a least-squares fit to the observed neutron line-integrals. Even when the elongation for the peripheral bounding surface is treated as a free parameter, it is still found to differ little from that for the core elongation.

6.4 THE ALPHA-HEATING EXPERIMENT

A key experiment (Thomas *et al* 1998) during the DTE1 campaign involved a sequence of five otherwise similar beam-heated discharges in which the deuterium to tritium density ratio was varied from pure deuterium to nearly pure tritium. Considerable care was taken with wall conditioning, to ensure that the wall recycling composition matched the fuel ratio of the beams. Consequently, the d:t fuel concentration ratio is expected to be flat across the plasma column. The objective was to examine the effectiveness of alpha-particle heating. This sequence of discharges was of interest for testing the NEPAM code because of the variation in angular momentum input from 80 keV deuteron beams to 160 keV tritium beams. No untoward features related to angular momentum input were uncovered. Thus, present interest is restricted to the performance of one of the highest yield discharges (# 42847).

Discharge # 42847 will be described in detail, to highlight some relevant features of the NEPAM code. The code was first run in simple modelling mode, resulting in a 30% under-estimate of the peak neutron emission (not, perhaps, of great concern in view of the discussion in section 5). More worrying, however, was the estimate of 75% of the neutron yield being emitted from the core volume, instead of the 65% indicated by the neutron profile monitor. Obvious candidates are the tritium concentration and Zeff. However, modest changes to the edge tritium concentration (about 70%, indicated by two different diagnostics) altered neither the total neutron yield nor the core neutron fraction. A preliminary pass of the predictive calculation was made at this point, as described below, to ensure that the cross-field transport provided a realistic estimate of the core tritium

concentration. The CXSM-derived Zeff was quite low (1.5 over the core volume), leaving no scope for adjusting the core neutron fraction in the desired direction. Changing the electron density profile, however, easily provided the required core neutron fraction. As the line-integrated electron density is accurately measured by interferometry, a reduction in core density must presumably be compensated by a rise in peripheral volume density. A 5% flattening of the density profile sufficed, which is within the experimental uncertainties. In short, a few minor data adjustments were made that led to the neutron yield being faithfully modelled. This is important for studies of the neutron energy spectrum (see section 6.7).

The predictive temperature calculation was run next, starting with the ohmic heating phase preceding the application of the beams for which ion temperature profile data are not available. The JH_c and JH_p factors were adjusted until the calculated and measured electron temperature and neutron emission were in satisfactory agreement prior to the commencement of beam heating, in order to define the target plasma correctly. The beam-injection period itself was then studied: the other two numerical factors $Frot_c$ and $Frot_p$ were adjusted until the global energy balance and the ion and electron temperature data were reproduced satisfactorily. With the ion temperature data satisfactorily reproduced, it was found that the computed electron temperature fell between the ECE and LIDAR temperature data. The acceptable reproduction of the experimental temperatures (figs. 17 and 18) assured the accurate prediction of the global neutron emission (fig. 19) and of the associated neutron profile data. The alpha-particle heating contribution only becomes noticeable after 13.2 s (the alpha-particle slowing down time is about 1.0 s). Fitting the empirical temperature evolutions demands either (i) the inclusion of alpha-particle heating effects or (ii) the adoption of an $Frot_c$ multiplier that is time-dependent; such a time-dependence is unnecessary for the low fusion yield discharges in the alpha-particle heating experiment and, in general, is never used. The NEPAM-calculated and the YAPAN-derived fractions of the neutron emission associated with the core volume are compared in fig. 20.

Having successfully reproduced the neutron emission, we can establish the maximum possible contribution of the fusion alpha particles to ion and electron heating simply by turning off the heating term in the calculation. Choosing the moment when the ion temperature (Ti) is at its maximum (14.0 s), we find Ti falls from 12.40 to 11.80 keV on switching off alpha heating, whereas the electron temperature (Te) falls from 9.06 to 8.32 keV. Thus the alpha contribution to the core temperature is just 0.60 keV for ions and 0.74 keV for electrons, for 1.27 MW of alpha-particle power. The careful analysis of Thomas *et al* 1998 indicated the contribution to electron heating was 1.3 ± 0.23 keV, for 1.3 MW of alpha-particle power, but referring to the axial electron temperature as measured by ECE. To make the appropriate comparison, we have to recognize that the ECE core-averaged temperature is higher than the LIDAR temperature (9.49 keV instead of 8.65 keV and, moreover, the ECE axial to core averaged peaking factor is also higher (1.26 instead of 1.06). Our estimate of the axial electron temperature contribution from alpha particle heating as measured by ECE is then 1.03 keV on axis, which is in fair agreement with the result of Thomas *et al*.

We conclude that the alpha particles appear to heat the plasma as expected, with no evident degradation due to MHD effects. This finding relates to temperature profiles that have been averaged over a core volume large enough to encompass about 60% of the neutron emission. Almost identical results were obtained from discharge # 42586, also with nearly equal deuterium and tritium concentrations.

6.5 THE RECORD FUSION POWER D-T DISCHARGE

The d-t discharge that produced the record fusion power is of particular interest, not least because of the difficulty experienced in modelling the neutron yield successfully. This discharge, # 42976, achieved a peak fusion power of 16 MW (5.7×10^{18} n.s^{-1}), although only transiently (Keilhacker 1999). The discharge was run with 4.0 MA plasma current and 3.7 T toroidal field. The plasma was initially fuelled during the ohmic heating phase with approximately 50:50 d:t gas mixture to condition the vessel walls, then the X-point magnetic configuration was established to reduce the plasma electron density prior to switching on the beam heating (nearly equal powers of deuterium and tritium injection) and the ICRF heating (3 MW, tuned to hydrogen). A full set of diagnostic measurements was available (Maas *et al* 1999). However, when calculating the expected neutron emission from the unmodified measured data, it was found that the calculated emission at beam turn-on rose appreciably faster than the measured data, thereafter the emission fell unduly rapidly and failed to attain the measured peak value. However, the core neutron fraction was in good agreement with the profile monitor data. An attempt was made to establish the source of the discrepancy by making reasonable normalization adjustments to all elements of the input data in turn, apart from Zeff, but without success. After investigating these potential defects, attention turned to the Zeff data.

Two sets of Zeff measurements are available; the spatially averaged data based on bremsstrahlung measurements and the CXRS profile data. In this case, the bremsstrahlung Zeff results (~ 3.0) are double the CXRS results (~ 1.5), as is sometimes found with substantial additional heating powers. Since the CXRS data are obtained only during the beam-heating period, it was necessary to amalgamate the two sets of measurements. In this case, the bremsstrahlung Zeff data, normalized to 15% above the absolute value given by the CXRS data, were adopted for the peripheral Zeff. The NEPAM code was used to deduce the core Zeff; the resulting core Zeff values were somewhat below the CXRS values and were responsible for the improved fit to the measured peak neutron yield. The breakdown of the neutron emission into its component parts is shown in fig. 21, where the initial over-prediction is seen. The calculated and measured yields can, of course, be brought into perfect agreement for the period 12.1 to 12.7 seconds by suitably modifying Zeff but the necessary adjustments are unreasonable as they lie well outside the uncertainties associated with the actual measured data.

The calculated neutron yields shown in fig. 21 are based on computed ion temperatures so that the post beam-heating period can be examined. Some undesirable ambiguity for the temperature

calculation is introduced by the use of RF heating. The usual assumption is that half the ICRF power is retained in the core, where it drives a high-energy proton tail until the ion temperature rises above 15 keV, after which bulk ion heating is assumed (as a simplification for second harmonic heating of deuterium). In this way, both ion and ECE electron temperatures are well reproduced during the beam-heating phase. Second harmonic acceleration of deuterium at the higher temperatures might be expected to generate a non-thermal tail that would contribute directly to the neutron emission but calculations show that this could never be large enough to be important (for discharge # 42976).

Excellent agreement between the calculated and measured core neutron yield fractions was obtained. Indeed, the computed neutron emission profiles agree very well with the measured profiles, provided the computed yields are normalized to the measured yields, which is quite a large adjustment (a factor of 0.6) at early times into the discharge.

Other selected d-t discharges without RF heating have been examined for this exaggerated neutron yield in the rise phase but, where encountered, it always proved to be an easy matter to adjust the input data (usually Zeff or the recycling t:d ratio) within experimental errors so as to resolve the issue.

6.6 AN OPTIMIZED SHEAR DISCHARGE

The modelling of optimized shear discharges is particularly interesting because of the existence of the internal transport barrier and associated radial electric fields that could perturb the plasma rotation rate and so violate the momentum conservation calculation used in the NEPAM code. The use of lower-hybrid current (LHCD) drive to produce a plasma current with reversed-shear causes the ECE and LIDAR electron temperatures to disagree during the LHCD period. The application of significant ICRF heating power is potentially problematic as it can produce effects that are far more complex than are simulated in the code but normally the ICRF power level used in optimized shear discharges is restricted to just a few MW. Some difficulty arises from the uncertainties associated with the experimental data, as the spatial resolutions are coarse compared with the dimensions of the neutron emitting core volume - which can fall to 6 m^3. For such discharges, our problems start with the neutron profile monitor data, which possesses too few channels to define precisely the emission from the plasma centre when the emission is so highly peaked. However, discharge # 51976 is one of the highest yield optimized-shear discharges and happens to be suitable for analysis because the core volume does not fall below 9 m^3. Even so, the profile monitor analysis code (YAPAN) performs poorly during the final second of the discharge, when the central transport barrier is well established, possibly because the shape of the neutron-emitting region becomes triangular rather than elliptical as assumed.

When NEPAM was run for discharge # 51976 using measured temperatures, it was found that the total neutron emission was reproduced adequately provided the CXRS Zeff data were raised by 50%. The core neutron fraction is fairly constant at about 75% instead of the 63% indicated by YAPAN (apart from the last second of the discharge). In principle, it should be possible to adjust the normalization factors of the relevant diagnostic measurements until the correct core neutron

fraction is achieved; however, this proved not to be an easy matter. The code was next run with computed temperatures. The previously adjusted core and peripheral Zeff were adopted. $Frot_c$ was left set to 1.0 throughout, as this value proved adequate. The ICRF heating power (4.0 MW) was divided almost equally between the core and the peripheral volumes, as usual, and the $Frot_p$ factor was set to 0.5, as required to bring the peripheral temperatures close to the measured values. The RF heating was assumed initially to drive a fast proton distribution with effective energy of 300 keV in the core and 30 keV in the periphery. The results are not sensitive to the precise values chosen. Once the ion temperature had risen above 15 keV, the core heating was transferred to bulk ion heating to simulate 2^{nd} harmonic heating of deuterons; this was essential - and customary - to reproduce the observed ion temperature time dependence. The results of this procedure are shown in figs. 22 - 24. Not shown is the core neutron fraction, which was little different from that obtained using measured temperatures. As shown in fig. 22, the calculated ion temperatures agree remarkably well with the measured temperatures. The ECE and LIDAR electron measurements, fig. 23, differ by about 20%, with the ECE values being greater as usual at high temperatures. The calculated electron temperatures tend to fall between the two sets of measured data, and the calculated global neutron yields, fig. 24, are in very good agreement with the measured data. At peak emission, the neutron emission is seen to rise to 75% thermal, a very high value. The core JH_c factor falls close to zero during the final 1 second of the discharge, indicating no particle fuelling of the core from the peripheral region, as expected when a strong transport barrier exists. The barrier is one-sided, however, since the core particle confinement time never rises above 0.75 s. Running the calculation without the ICRF heating shows the thermal emission to be halved.

6.7 INTERPRETATION OF NEUTRON ENERGY SPECTRA

A range of neutron spectrometers has been deployed at JET, for operation in d-d and d-t plasmas (Jarvis 2002). The type of neutron energy spectrum analysis that has to be used is dependent on the plasma heating techniques employed. For example, with ohmically heated plasmas the neutron spectrum is closely gaussian in shape and the spectrum width provides an accurate measurement of the core temperature. However, high performance discharges all employ neutral beam heating with, possibly, simultaneous ICRF heating. In such cases, the interpretation of the neutron spectra becomes complex, though tractable (Hawkes *et al* 2002a, Krasilnikov *et al* 2002). In this section, we return to the beam-heated d-t discharge # 42847 as an example of the comparison of predicted with measured neutron spectra, using the annular-radiator spectrometer (Hawkes *et al* 2002b) that has a quasi-tangential view of the plasma. Such a view is sensitive to the plasma rotation rate and the fitting of a computed spectrum to the measured spectrum is far more difficult than for a spectrometer that enjoys a radial view, and which is therefore insensitive to the toroidal motion of the reacting ions.

A full calculation of a predicted neutron spectrum should involve a large number of individual calculations for a series of small volume elements along the spectrometer line-of-sight. However, because the neutron emission is so strongly peaked towards the centre, the problem is amenable to

simplification. In the past (Elevant *et al* 1995), the adoption of a single volume element has proven reasonably successful for d-d plasma discharges. Consequently, we would expect the NEPAM two-volume calculation to be entirely adequate. The code provides a breakdown of the reactions contributing to the total neutron emission from both the plasma core and the periphery. In the core, we have to take into account the thermal neutron yield and the d-t and t-d beam-plasma yields. The beam-plasma emissions are dominated by the full-energy component of the injected neutral beams, but the 1/2 and 1/3 energy components should not be ignored. The beam-beam component is only important at early times in the discharge, before the temperature has risen. As described in section 6.4, the deuterium to tritium ratio in the plasma core was established by adjusting $Frot_c$ and $Frot_p$ until the plasma effective ion and electron temperatures calculated by NEPAM reproduced the measured data.

Provided injected fast ions remain on their deposition flux surfaces, the co:counter ratio can be easily estimated: in the core, the fast ions move predominantly (90%) in the co-direction whereas in the periphery the beam trapping is strong and almost equal numbers of fast ions move in co- and counter-directions. Beam particles that are on predominantly passing orbits just after ionization will remain so if pitch-angle scattering and cross-field diffusion are unimportant. Provided this is the case, then the core and peripheral region spectra are the simple sums of just three components (deuterium beam - thermal tritium, tritium beam - thermal deuterium and thermal-thermal reactions), of which the deuterium and tritium beam components have to be computed with a Monte-Carlo kinematics code FPS (van Belle and Sadler 1986) for the beam injection angle, the neutron spectrometer viewing direction, and the components of the rotation speed along the spectrometer line-of-sight as computed with NEPAM. FPS computes the neutron spectrum for all injected particles of a given species in a single run, e.g. for both 78 keV and 142 keV deuterium beams and their one-half and one-third energy components in specified proportions; it also includes both co- and counter-passing ions as needed and performs a simple pitch-angle scattering calculation.

The spectrometer views the plasma along a horizontal chord through the plasma of 10-cm diameter, passes 15 cm below the nominal plasma mid-plane. The chord is quasi-tangential, subtending an angle of 52^o to the toroidal field lines at the centre of the plasma column. Since the majority of the trapped-particles have end-points that fall well away from the mid-plane, it is assumed that the trapped orbits from which neutron emission is sampled are adequately represented by their ionization pitch-angles. Such an approximation would not be appropriate for a spectrometer viewing a complete vertical section of plasma. The present calculation is thereby reduced to just a total of 6 components: three each, for both core and periphery. All of these components have to be summed, again using relative weightings provided by NEPAM. Finally, the spectrometer response function has to be folded into the computed neutron spectrum for comparison with the measured spectrometer response, which in the present example records knock-on protons scattered at a forwards angle of about 20^o.

Fig. 25 shows the comparison of the computed and measured neutron spectra for the time interval 14 to 14.5 s. The computed neutron energy spectrum is shown in the lower panel. The core contributes

64% of the total neutron emission. 54% of the contribution from the core is due to thermal reactions, the line-averaged ion temperature being 14-keV and the projection of the plasma speed (due to rotation) in the direction of the spectrometer is 3.0×10^5 m.s^{-1}. The deuterium beam-plasma emission is 1.5 times the tritium beam-plasma contribution in magnitude. The co:counter fast ion streaming ratio is calculated to be 11:1, neglecting pitch angle scattering, etc. The periphery contributes 34% of the total neutron emission. Only 31% of the peripheral emission is thermal, the ion temperature being 6 keV and the projected speed due to rotation 1.3×10^5 m.s^{-1}. The deuterium beam-plasma contribution is again greater than the tritium contribution and the co:counter ratio is calculated to be 1.7:1. The top panel of fig. 25 shows the measured recoil proton energy spectrum compared with the computed neutron spectrum folded into the spectrometer response function. (Unfortunately, the calculated spectrometer response function does not allow for the low energy tail that is presumably due to neutron down-scattering in the collimation). A very good fit between prediction and measurement has been obtained, with only minor adjustments. A least squares fitting procedure is available for adjusting all the neutron components simultaneously, if desired. In fact, only two quantities were adjusted to obtain the best fit. First, the absolute efficiency of the spectrometer was treated as a free variable as precision neutron collimation and window scattering and transmission calculations have not been performed. Secondly, the exact energy calibration of the spectrometer is regarded as another parameter that may be adjusted within the experimental uncertainty of about ± 30 keV, although in this instance the energy shift was only 15 keV.

The above prescription for computing the position and shape of the neutron spectrum is rather involved, but even so must be regarded as approximate. For this particular spectrum, it would appear that the computed fast ion co:counter passing ratios are consistent with the shape of the neutron energy spectrum, but the core beam-plasma neutron production relative to the total is too weak to justify a more detailed investigation. The neutron spectrum acquired over the first second of beam heating would be more suited to a study of the co:counter passing ratio as the thermal contribution is then small, although the beam-beam contribution is no longer negligible. Unfortunately, this spectrum contains rather few counts. Nevertheless, both the width and position of the calculated neutron spectrum are dependent on the co:counter passing fraction used in the FPS calculations and it is found that a ratio of 1:1 provides a better fit of the calculated to the measured spectrum than does the 16:1 ratio computed from the beam deposition profiles. This result shows the need for further refinements in the modelling.

7. CONCLUSIONS

This paper has described the use of the computer code NEPAM, its two related codes YAPAN and PLASMATH, and the kinematics code FPS which together permit the neutron emission to be computed from the available diagnostic data. When all the relevant diagnostic information is available, the neutron emission can modelled as accurately as with other codes. A distinctive feature is the ability to compute, for beam-heated discharges, the ion and electron temperatures from

knowledge of the plasma density and rotation rate profiles. Using just two normalization constants, the computed and measured temperatures can be brought into very close agreement for beam-heated discharges. Once this has been accomplished, the cross-field transport of fuel and impurity ions appears to be well simulated, as demonstrated most clearly in the trace-tritium gas injection experiment.

The main code, NEPAM, models the plasma using just two volume elements. That this proves adequate is due to the neutron emission being strongly peaked at the plasma centre and also to the use of the neutron emission profile to define the core volume. The core volume is a time-dependent quantity that responds to plasma performance changes, automatically including MHD events such as sawtooth crashes. The reconstructed profiles correspond surprisingly well with the measured profiles.

The code can be used to examine the consistency of the diagnostic data with the observed neutron emission and can be applied to a variety of interesting problems, being particularly useful where important experimental data are missing. For example, its ability to predict the D:T fuel mix in the core from measurements made at the edge is of considerable value for discharges with 14-MeV d-t neutron emission. Accordingly, the various examples in this paper have emphasized the d-t experiments, covering triton burnup studies, the deduction of deuterium to tritium fuel concentrations in the plasma core from deuterium beam-blips, the trace-tritium transport experiment, the alpha-particle heating experiments and the specification of the relative strengths of beam-plasma and thermal fusion reaction processes needed for calculations of neutron energy spectra. The code can be applied to most types of discharge, although the neutron profile analysis routine encounters difficulties with optimized-shear discharges that have exceptionally small core volumes and argon and neon impurity puffing discharges prove unsatisfactory due to inadequate diagnosis of the impurity density profiles. Fuel ion populations that are significantly perturbed by ICRF-acceleration to suprathermal energies are only crudely simulated.

The underlying principle for the use of the code predictively is that cross-field transport is assumed to be predominantly macroscopic in nature. The observed relationship between plasma rotation rate and density is then interpreted through the application of classical conservation laws. That the consequent prediction of ion and electron temperatures for beam-heated discharges that reproduce accurately their experimentally-determined counterparts does depend on introducing two normalization factors, not far removed from unity, is hardly surprising in view of all the experimental uncertainties involved. Interestingly, these factors essentially affect only the combined normalization of the ion and electron temperatures, while their ratio is predicted more precisely. One clear, but possibly unexpected, conclusion is that the neutron emission from the core of a JET plasma discharge is strongly influenced by conditions at the plasma edge.

APPENDIX

.2 EXPANDED DESCRIPTION OF THE TRACKING AND HEATING CALCULATIONS

The tracking calculation, in which ion and electron densities, impurity levels and rotation rates are evolved using macroscopic cross-field transport, is most easily understood if introduced as an initial-value calculation that predicts these quantities for a hypothetical discharge. As the starting point for the calculation, a realistic set of plasma parameters is adopted for a given moment in time during the initial ohmic heating phase of a real or imagined discharge. In addition, the time-dependence of the applied additional heating power has to be specified, along with a representative H_ signal. Specifying the ratio of impurity ion influx to hydrogenic ion influx simulates the Zeff signal. Finally, estimated values are introduced for the two particle confinement times ($\__c$ and $\__p$) and for the two Johnson-Hinnov factors (JH_c and JH_p) for the plasma core and peripheral regions, respectively. For simplicity, these last four parameters would be constants although arbitrary time-dependencies could be imposed. The ensuing calculation would generate unique rotation-rate, particle density and Zeff time evolutions that could, if desired, be forced to simulate corresponding experimental measurements for an actual discharge by suitable manipulation of the input data.

The calculation proceeds from one time-step to the next by evaluating a large set of equations, one for each quantity of interest in both core and peripheral regions; these are the individual particle densities for fuel and impurity ions, the electron density, angular momentum for the region, Zeff, the Johnson-Hinnov factors, the particle confinement times, etc. The values for a given time-step are derived for each quantity from its value at the preceding time-step by adding the incremental changes appropriate to that time-step. For example, the angular momentum of the plasma core is deduced from its value in the preceding time-step by adding three contributions: (i) a momentum enhancement from deposited beam ions (assuming instant slowing down), (ii) another enhancement from the transfer of ions and electrons from the peripheral region, as specified by the product of the adopted JH_c factor and the H_ signal, (analogous to the usual atom influx due to wall recycling and gas puffing, except that here the transferred particle properties are those of the bulk peripheral region), (iii) a loss due to the particle outflow to the peripheral region in accord with the assumed particle confinement time. Since macroscopic transport is assumed, the appropriate proportion of impurity ions and associated electrons are simultaneously transferred. Similarly, all the core particle densities are enhanced by adding the deposited beam ions and electrons (as extra thermal particles) and are reduced in accordance with the adopted particle confinement time, these removed particles being placed in the periphery. Analogous adjustments are made for the peripheral region, bearing in mind the particle transfers to and from the core (already determined) as well as the recycling influx of ions (hydrogenic and impurity) and electrons from the vessel walls and the loss of particles as appropriate for the assumed particle confinement time for this region. This entire calculation generates time-dependencies for the hypothetical discharge that vary as smoothly as do the input data.

The next stage in the explanation is the imposition of the tracking requirements, with the measured rotation rates, electron densities and Zeff values being the target values that should be reproduced.

For each time-step and region, three intermediate calculations are run. First, the derived rotation rates are automatically adjusted to closely reproduce the target rotation rates by computing appropriate values for the parameters JH_c and JH_p. In order to minimize the inevitable tendency for oscillatory behaviour, the tracking algorithm prevents parameters derived in one time-step from changing dramatically from their previous values. Next, the derived electron densities are likewise adjusted to reproduce the target densities by calculating the appropriate values for $\_c$ and $\_p$. Finally, the impurity levels are adjusted so as to conform to the observed Zeff data. Within each sub-calculation, the mutual interdependencies between the derived parameters are ignored, so several time-steps are required for them to stabilize. This calculation reproduces the observed plasma parameters closely, provided very small time-bins are employed (e.g. 1 ms or smaller). Unfortunately, such small time-bins result in excess computer run times and lead to computational problems. Normally, time-bins of 10 or 20 ms are chosen, depending on discharge duration. However, for plasma discharges with particle confinement times as small as a few tens of milliseconds, the requirement for generating smoothly varying signals results in the target densities, rotation rates and Zeff values being missed by unacceptable amounts. Calculating the mismatch factors, scaling the target signals so that they lie even further away from the calculated values and re-running the entire calculation resolves this difficulty. This second pass is found to reproduce the desired signals adequately, without undue oscillatory behaviour.

In this way, the quantities that were stated in the opening paragraph to be pre-determined for purposes of explanation are provided as output signals derived uniquely from the actual calculation *during periods of beam heating*. Of course, they have to be adjusted manually in the event of their experimental counterparts not being available (e.g. no measured rotation rates or ion temperatures). In particular, JH_c and JH_p have to be adjusted manually (i.e. to reproduce the measured neutron data) during the periods of at least 0.5s of ohmic heating that is always modelled before and after the application of beam heating.

A number of minor complications arise once the core and peripheral volumes are permitted to become time-dependent; these involve making further plasma exchanges from one region to the other. Care is taken throughout to ensure angular momentum conservation, particle conservation and charge neutrality. In passing, we note that the measured neutron emission tends to be reproduced more faithfully when the calculation is allowed to determine the core Zeff directly from the peripheral Zeff, instead of having the empirical core values imposed.

The tracking and heating calculations should performed simultaneously but doing this causes an unacceptable increase in computer running time for lengthy discharges (i.e. longer than 10 s). Instead, the heating calculation is run after the tracking calculation has been completed. The heating calculation is straightforward in so far as there are no unknown quantities remaining at this stage. However, it is now necessary to distinguish fast and thermal ion densities. The beam and RF-accelerated fast ions are caused to slow down classically, using a multi-group representation, losing energy to both thermal ions and electrons on a time-bin-by-time-bin basis. When thermalized, the

ions are added to the thermal background. The predetermined Johnson-Hinnov factors and particle confinement times are employed and the total densities (fast plus thermal) reproduce the (thermal) densities generated by the tracking routine. The cross-field transport is restricted to thermal particles. Classical ion and electron energy equipartition rates are adopted for the thermal particles within each region.

The ion and electron temperatures resulting from the heating calculation are now available for comparison with the corresponding experimental values for the core and peripheral regions. No deliberate mechanism has been provided for adjusting the ratio of the calculated ion to electron temperatures (none has been found necessary). However, we note that this ratio is somewhat affected by the identities and abundances of the impurity ions, although these are generally well known. Should the calculated and measured temperatures differ significantly, they can be brought into agreement by suitable choices of the two adjustable constants $Frot_c$ and $Frot_p$ that are near unity multipliers of the momentum deposited by the beam ions. This involves a manual intervention and re-running the whole calculation.

Tests have shown that very similar results are obtained regardless of whether the tracking and heating calculations are combined or run separately. The use of instant stopping of beam ions in the tracking routine might be considered problematic. Calculations performed for the core region using gradual slowing of the beam ions have shown that the resulting rotation rate is only marginally greater than that calculated with promptly stopping ions, and then only during the early moments of the acceleration phase at beam switch-on. (With gradual stopping, the mass of the slowing down ion is not added to the thermal bulk until it enters the thermal energy group). For the peripheral region, where most of the beam ions are injected into trapped orbits, the prompt stopping approximation is a more appropriate choice than gradual stopping. Another problem concerns the tracking routine treatment of the fast ions in the plasma core as if thermal, despite the fact that the fast ion content can be a significant fraction of the whole. The measured rotation rate is, essentially, a property of the thermal ions alone. However, as the main issue for the tracking calculation is that of momentum conservation, the particle numbers transferred between core and periphery are unaffected by presence of the "spectator" fast ion population. Tests with the tracking and heating calculations combined have shown that they may be run consecutively without noticeable loss of accuracy.

ACKNOWLEDGEMENTS

The authors gratefully acknowledge contributions, made directly and indirectly, by various members of the former JET experimental and theoretical divisions, including P. van Belle, W.G.F.Core, V.Kiptily, F.B.Marcus, G.J.Sadler and K-D.Zastrow. This work was partly carried out under the framework of the JET Joint Undertaking and more recently under the European Fusion Development Agreement and was partly funded by EURATOM and the U.K. Department of Trade and Industry.

REFERENCES

[1]. Adams J M, Jarvis O N, Sadler G J, Syme D B and Watkins N 1993 *Nucl. Instrum. Methods* **A329** 277

[2]. Bosch H-S and Hale G M 1992, *Nucl. Fusion* **32** 611

[3]. Budny R V *et al* 1992, *Nucl. Fusion* **32** 429

[4]. Core W G F and Zastrow K-D 1996, JET Joint Undertaking Report JET-R96(01)

[5]. Costley A E, *Diagnostics for Contemporary Fusion Experiments", (Societa Italiana di Fisica, 1991)* p 223

[6]. Elevant T, van Belle P, Jarvis O N, Sadler G 1995, Nucl. Instrum. Methods, **A364** 333

[7]. Ericksson L-G, Hellsten T and Willen U 1993, *Nucl. Fusion* **33** 1037

[8]. Giroud C 2001 (priv. comm.)

[9]. Gowers C 1991, *Diagnostics for Contemporary Fusion Experiments, (Societa Italiana di Fisica, 1991),* p 243

[10]. Greenwald M *et al* 1988, *Nucl. Fusion* **28** 2188

[11]. Hawkes N P, Bond D S, Kiptily V, Jarvis O N, Conroy S W 2002a, *Nucl. Instrum. Methods in Phys. Res.* **A 476** 490

[12]. Hawkes N P, Bond D S, Croft S, Jarvis O N and Sherwood A C 2002b, *Nucl. Instrum. Methods in Phys. Res.* **A 476** 506

[13]. Hinton F L and Rosenbluth M N 1999, *Physics Letters* **A 259** 267

[14]. JET Team (prepared by K-D. Zastrow) 1999, *Nucl. Fusion* **39** 1891

[15]. Jarvis O N, Clipsham E, Hone M, Laundy B, Pillon M, Rapisarda M, Sadler G, van Belle P and Verschuur K A 1991, *Fusion Technol.* **20** 265

[16]. Jarvis O N, Adams J M, Howarth P J A, Marcus F B, Righi E, Sadler G, Start D F H, van Belle P, Warrick C and Watkins N 1996 *Nucl. Fusion* **36** 1513

[17]. Jarvis O N 1997, *Plasma Phys. Control. Fusion* **39** 1571

[18]. Jarvis O N, Adams J M, Marcus F B and Sadler G J 1997, *Fusion Eng. Design* **34 - 35** 59

[19]. Jarvis O N, Balet B, Ehrenberg J K, Guenther K, Howman A C, von Hellermann M G, Morgan P D, Stamp M, Zastrow K-D 1998, *Proc. 1998 Int. Congress on Plasma Phys. & 25th Eur. Phys. Soc. Conf. on Contr. Fusion and Plasma Physics, (Prague, 1998). Europhys. Conf. Abstr.* **22C** 389

[20]. Jarvis O N 2002, *Nucl. Instrum. Methods in Phys. Res.* **A 476** 474

[21]. Johnson L C and Hinnov E 1973, J.Quant. Spectrosc. Radiat. Transfer ***13*** 333

[22]. Keilhacker M, Gibson A, Gormezano C *et al* and the JET Team 1999, *Nucl. Fusion* **39** 209

[23]. Krasilnikov A V, Amosov V N, van Belle P, Jarvis O N, Sadler G J, 2002, *Nucl. Instrum. Methods in Phys. Res.* **A 476** 500

[24]. Maas A C, Andrew P, Coad P, Edwards A, Ehrenberg A *et al* 1999, *Fusion Eng. Design* **47** 247

[24]. Mandl W, Wolf R, von Hellermann M, Summers H P 1993, *Plasma Phys. Control. Fusion* **35** 1373

[25]. Matthews G F, Zastrow K-D, Andrew P, Balet B, Basse N P, Ehrenberg J et al 1999, *J. Nucl. Materials* **226-269** 1134
[26]. O'Brien D P *et al* 1992, *Nucl. Fusion* **32** 1351
[27]. Spitzer L 1962, Jnr, *Physics of Fully Ionized Gases, 2nd Ed.,* (New York: Interscience)
[28]. Stix T H 1972, *Plasma Physics* **14** 367
[29]. Thomas P R, Andrew P, Balet B, Bartlett D, Bull J, de Esch B, Gibson A *et al* 1998, *Phys. Rev. Letters* **80** 5548
[30]. van Belle P and Sadler G J1986, *Basic and Advanced Diagnostic Techniques for Fusion Plasmas (Varenna,1986)* vol. III (EUR 10797 EN) (Brussels: CEC) p 767
[31]. von Hellermann M, Core W G F, Howman A, Juper C, Konig R W T , Stamp M F, [1].
[32]. Summers H P, Thomas P R and Zastrow K-D 1996a *Diagnostics for Experimental Thermonuclear Reactors (New York: Plenum Press, 1996)* p.321
[33]. von Hellermann M G *et al* 1996b, *Diagnostics for Experimental Thermonuclear Reactors (New York: Plenum Press, 1996)* p 281
[34]. Veron D 1982, *Diagnostics for Fusion Reactor Conditions, (ECSE-EEC-EAEC (Euratom), 1982),* p199
[35]. Wesson J 1997, *Tokamaks, Second Edition* (Oxford: Clarendon)
[36]. Zastrow K-D, Core W G F, Ericksson L-G, von Hellermann M G, Howman A C and [1].
[37]. Konig R W T 1998, *Nucl. Fusion* **38** 257

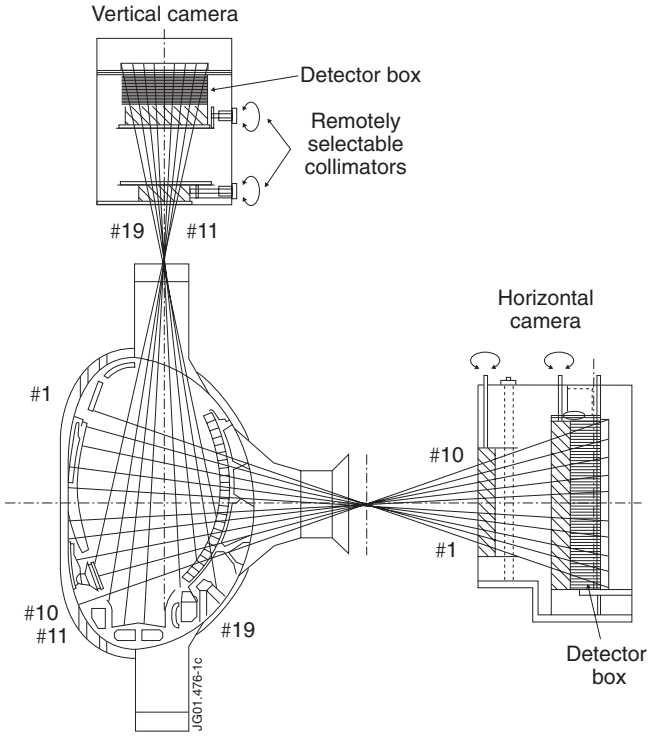

Fig.1: The JET neutron profile monitor. Note that the vertical (viewing) camera records the horizontal emissivity profile, etc. The channel numbers are indicated.

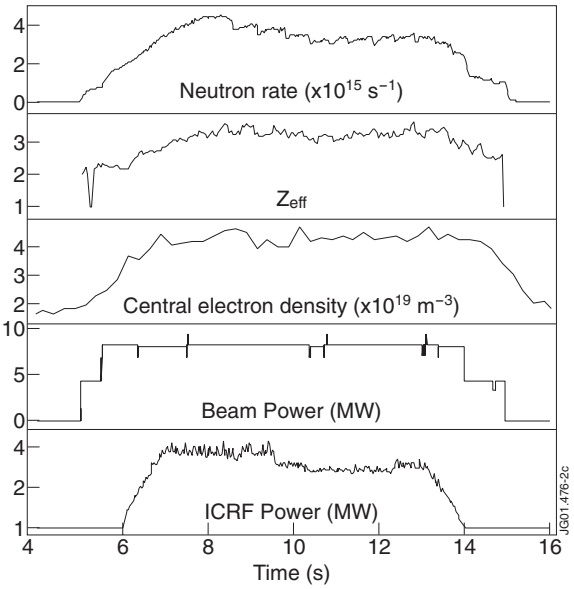

Fig. 2: Time traces for Pulse No: 50623, showing the neutron emission rate, average effective charge, central electron density, neutral beam heating power and the ICRF heating power.

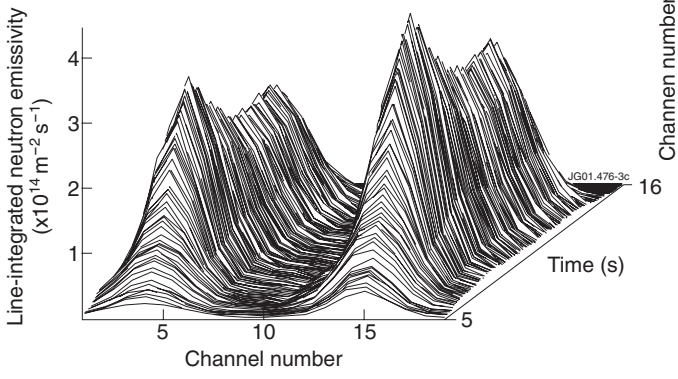

Fig. 3. A 3-D representation of the line-integrated neutron emission recorded with the 19-channel neutron profile monitor for Pulse No: 50623. Channel numbers 1 through 10 belong to the horizontal camera, 11 through 19 to the vertical camera.

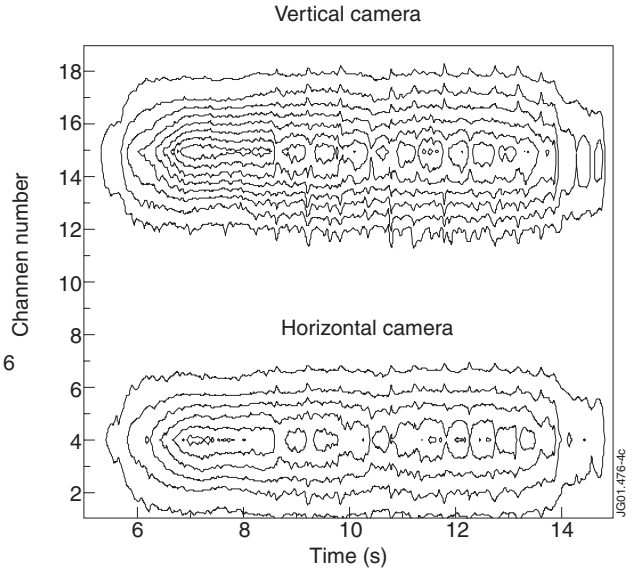

Fig. 4: Contour plot of the line-integrated neutron emission data shown in fig. 3. The profiles have been normalized to constant total neutron emission strength in order to emphasize the changes in profile shape. This form of plot shows the sawtooth crashes very clearly.

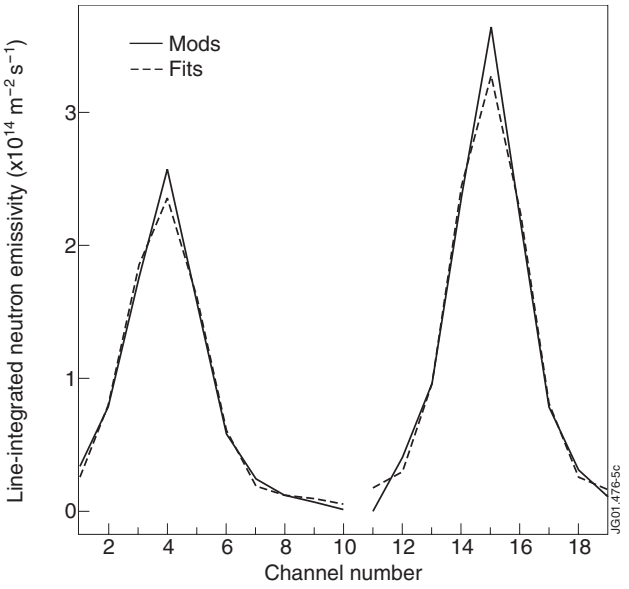

Fig. 5: Line integrated profiles at 7.0 seconds into Pulse No: 50623 for the horizontal (channels 1 - 10) and vertical (channels 11 - 19) cameras. The MODS curves represent the experimental profiles after normalization to the neutron yield given by the fission chambers, the FITS being the corresponding data reconstructed from the fitting procedure.

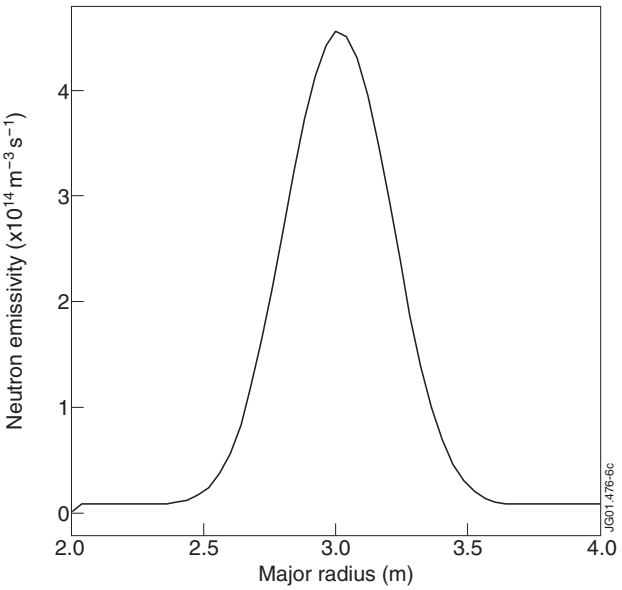

Fig. 6: The fitted neutron emissivity profile, projected along the major radius, at time 7.0 seconds into Pulse No: 50623.

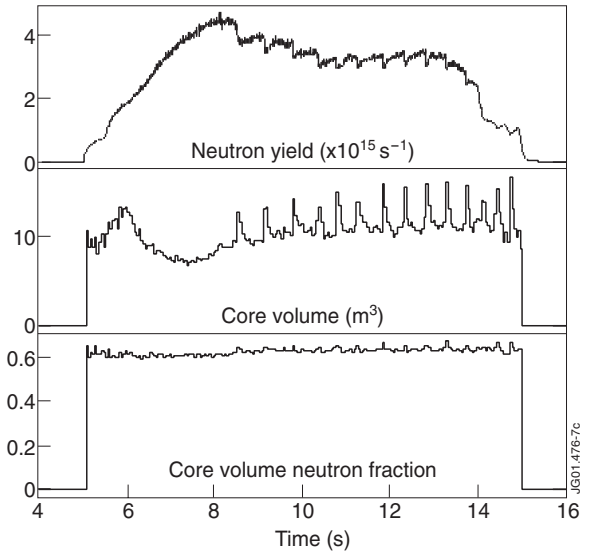

Fig. 7: The total neutron emission and the derived parameters that encapsulate the neutron emission profile data for Pulse No: 50623, namely the core volume and the core volume neutron fraction.

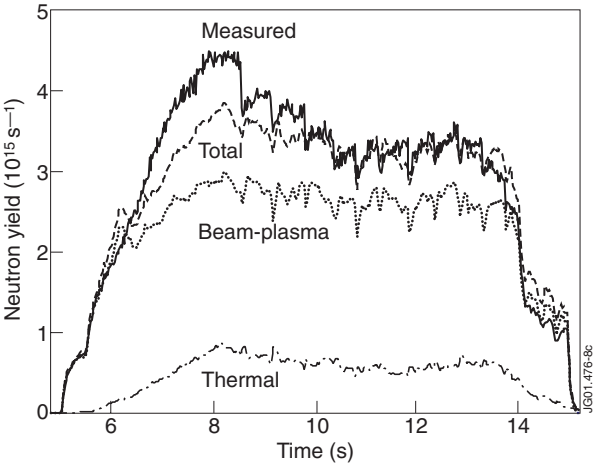

Fig. 8: Illustrating the agreement between the computed neutron yield and the measured yield for Pulse No: 50623. The break-down of the total yield into beam-plasma and thermal contributions is indicated. It is assumed that the ICRF heating accelerates protons but not deuterons.

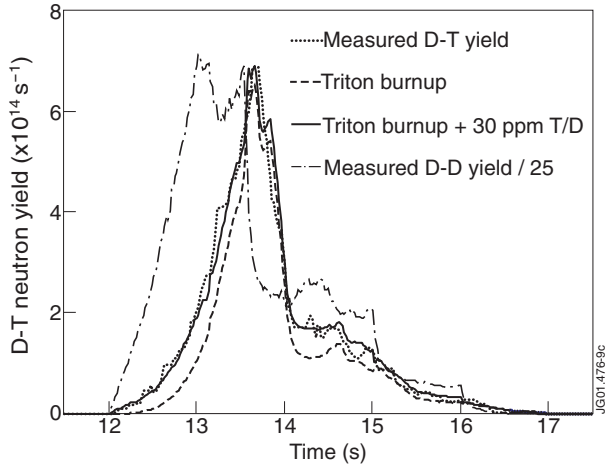

Fig. 9: Triton burnup calculation for 3.0 MA, 3.5 T Pulse No: 49755. This discharge was heated with 15 MW NBI. No CXRS ion temperature data were available, so the ion and electron temperatures had to be computed. The calculated 2.5MeV neutron yield reproduces the measured yield satisfactorily. In order to obtain the fit to the 14 MeV neutron signal, it was necessary to assume 30-ppm of residual tritium in the plasma.

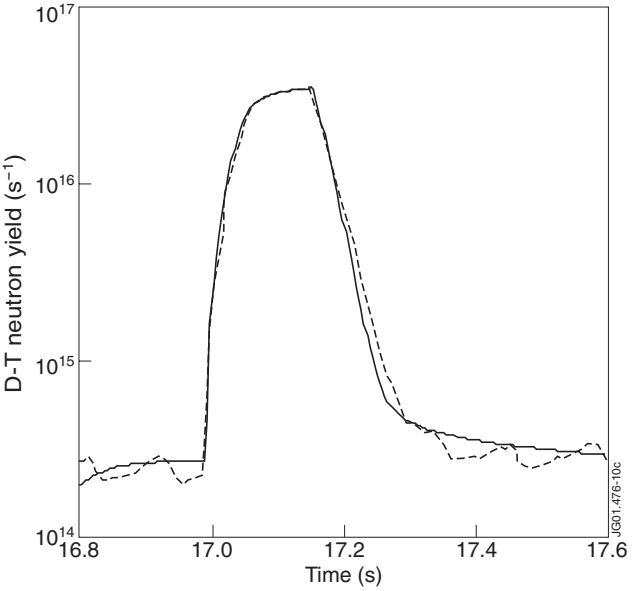

Fig. 10: Showing the increase in total neutron emission when a 1.2 MW 75 keV deuterium beam is injected into a 3 MA, 3.5T ohmic Pulse No: 41683 for 160 ms. The plasma contains 40% D and 60% T. The figure demonstrates the reliability of the beam slowing down calculation; the small discrepancy is within the experimental uncertainty of the electron temperature measurements. The predicted (solid curve) and measured yields (dashed) are brought into coincidence at peak intensity by adjusting the tritium concentration. Note that the neutron emission during the ohmic phases is also reproduced.

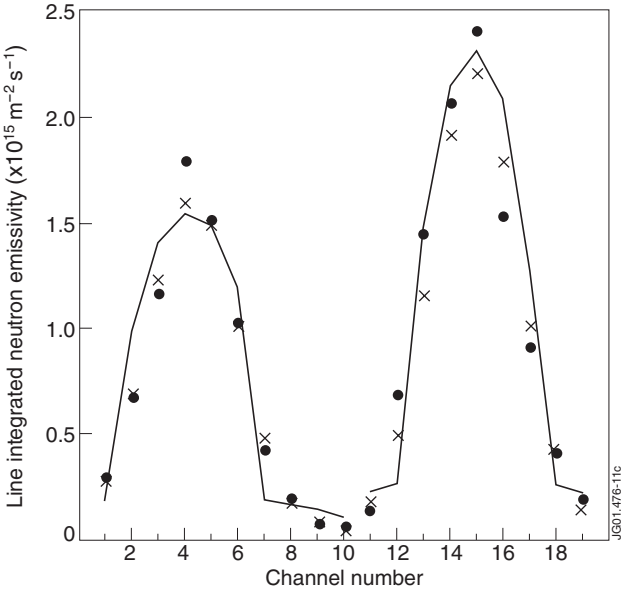

Fig. 11: The neutron emission profile corresponding to time 17.12 s for Pulse No: 41683 (see fig. 10). The line-integrated intensities are shown for all 19 channels of the two cameras. The solid circles are the measured line-integrals, the crosses are the improved line-integrals derived from the fitting programme and the line joins the corresponding values predicted by the NEPAM code. The abrupt changes in slope result from the use of a plasma model containing only two volume elements.

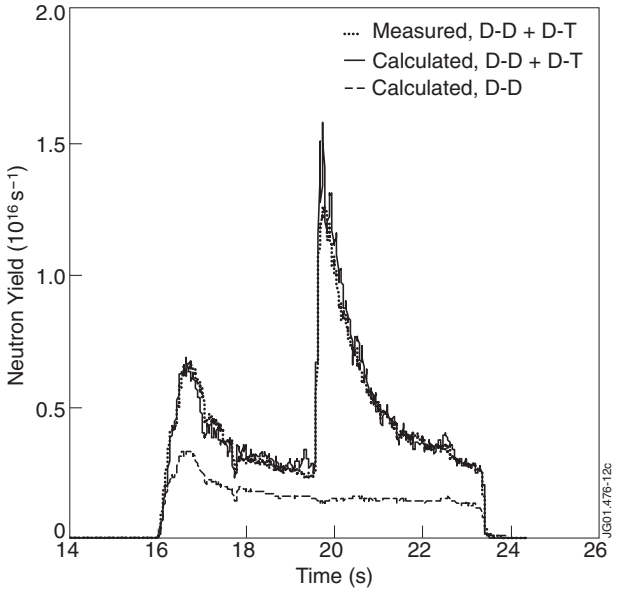

Fig. 12: D-D and D-T global neutron yields for Pulse No: 42531. The measured total yield (dotted line) is obtained from the fission chambers, which are insensitive to neutron energy. The profile monitor distinguishes d-d and d-t yields. The two other curves are calculated: d-d neutron yield (dashed) and the sum of the d-d and d-t yields (solid). The tritium recycling composition is adjusted until the calculated d-t yield agrees with the measured d-t yield.

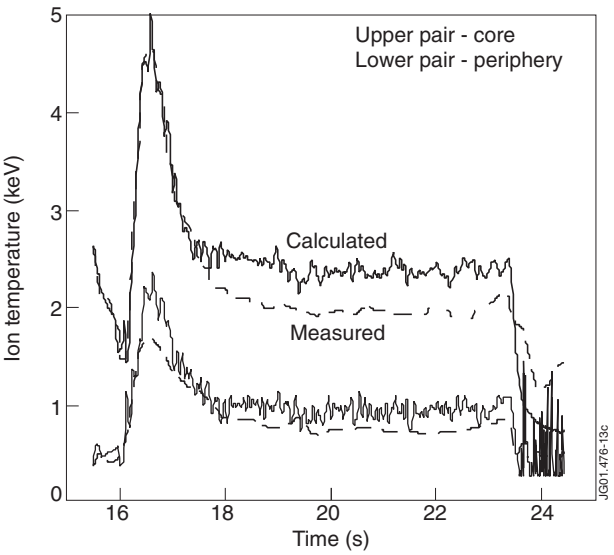

Fig. 13: Comparison of calculated with measured ion temperature data, averaged over the core and peripheral volumes, for Pulse No: 42531. See text for comments.

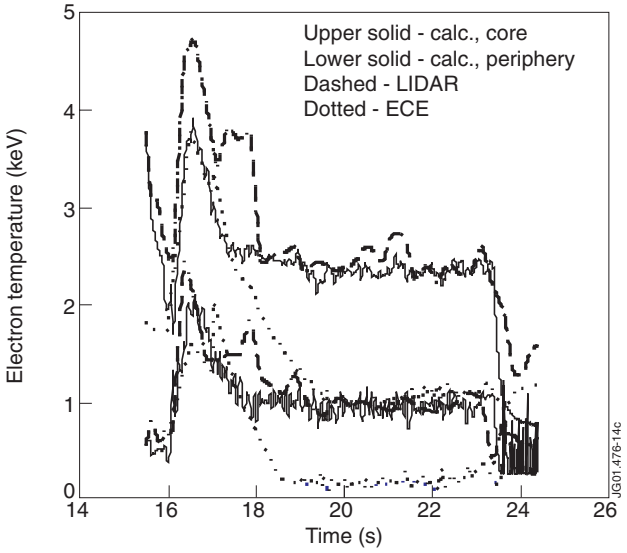

Fig. 14: Comparison of calculated with measured electron temperature data, averaged over the core and peripheral volumes, for Pulse No: 42531. See text for comments.

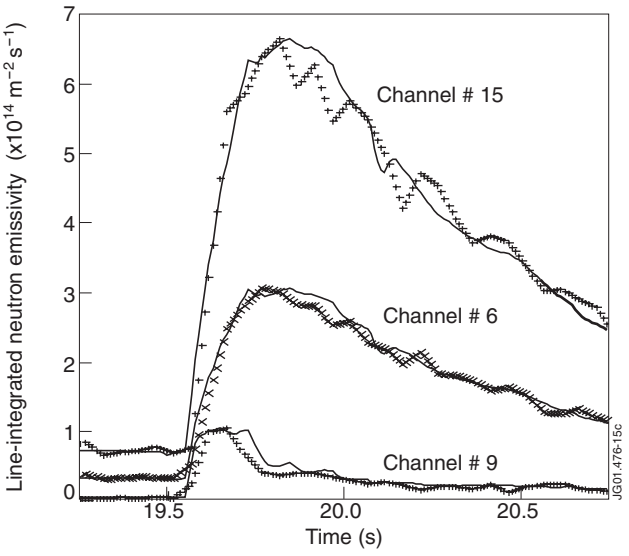

Fig. 15: Comparison of calculated line-integral data for three channels of the profile monitor, for Pulse No: 42531. Channels 6 and 15 correspond to nearly central views from the horizontal and vertical cameras, respectively. Channel 9 is the outer-most channel of the horizontal camera that gives a useable signal. The pairs of curves are normalized at their peak values, for comparison purposes.

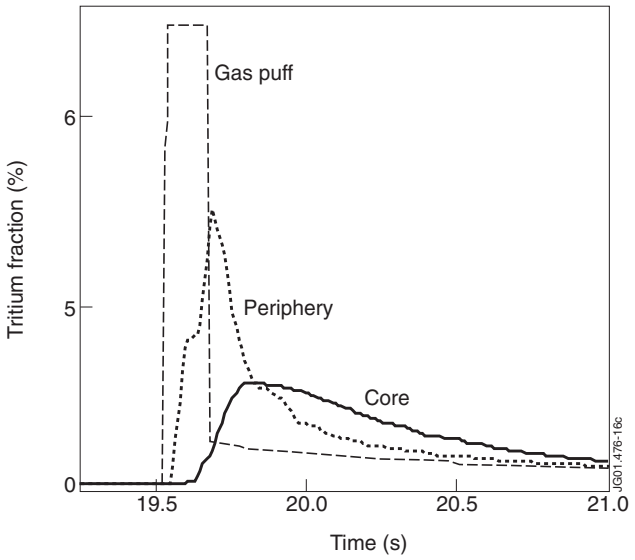

Fig. 16: Showing the assumed time-dependence of the tritium gas puff, and subsequent recycling. The calculated tritium compositions in the core and peripheral volumes are also shown. In order to derive estimates of the diffusion coefficients in these regions, it was necessary to re-run the calculation with influxes of tritium inhibited after the gas puff.

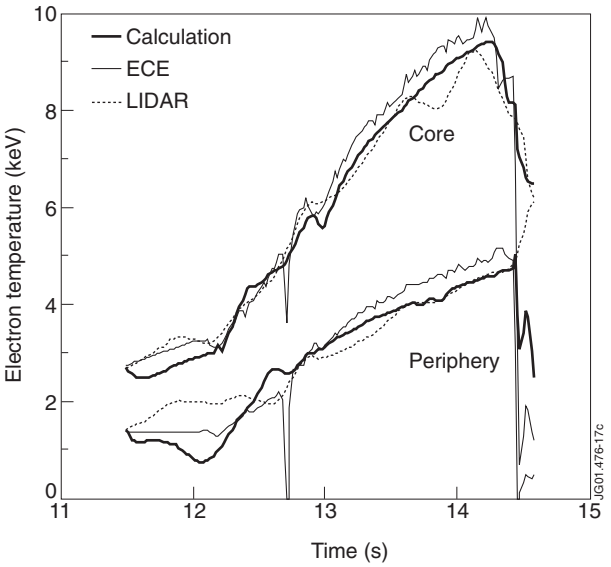

Fig. 17: Comparison of calculated (heavy lines) and measured electron temperatures (thin lines) for Pulse No: 42847, which was the highest performance discharge in the alpha-particle heating experiment. Note the minor spread between the ECE and LIDAR electron temperature data sets.

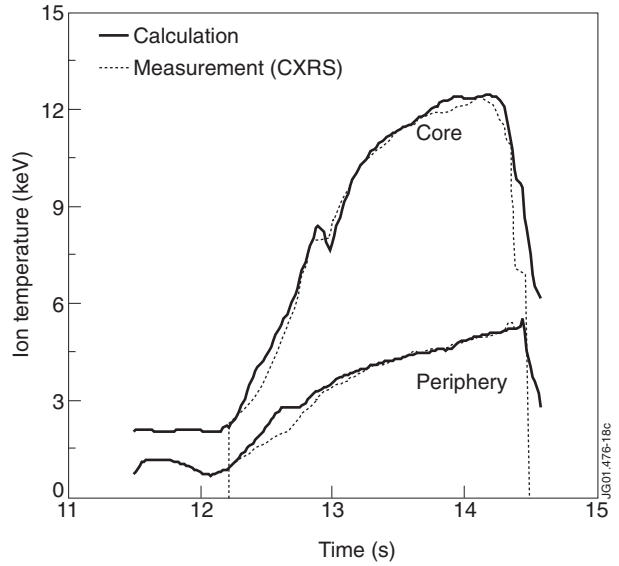

Fig. 18: Comparison of calculated (solid lines) and measured (dashed lines) ion temperatures for Pulse No: 42847, which was the highest performance discharge in the alpha-particle heating experiment. Although the agreement is excellent, the resulting neutron yield and profile can only be brought into agreement with measurements after adjustment of both electron density and Z_{eff} profile data.

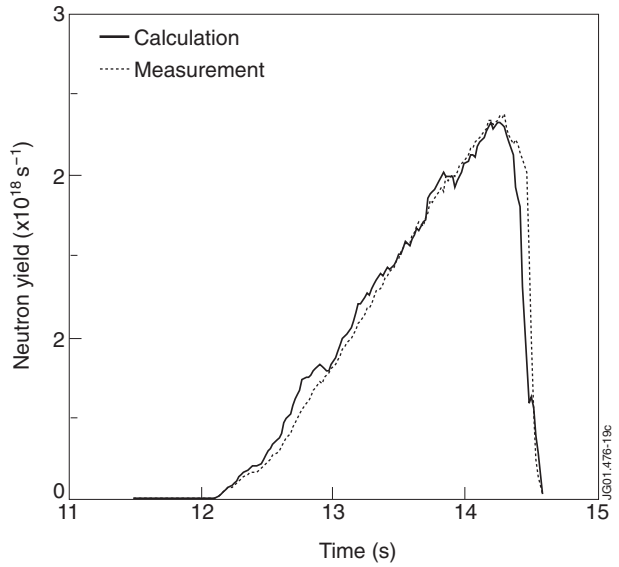

Fig. 19: Comparison of measured global neutron yield (dashed) for Pulse No: 42847, with the calculation (solid) employing the temperature data of figs. 17 and 18.

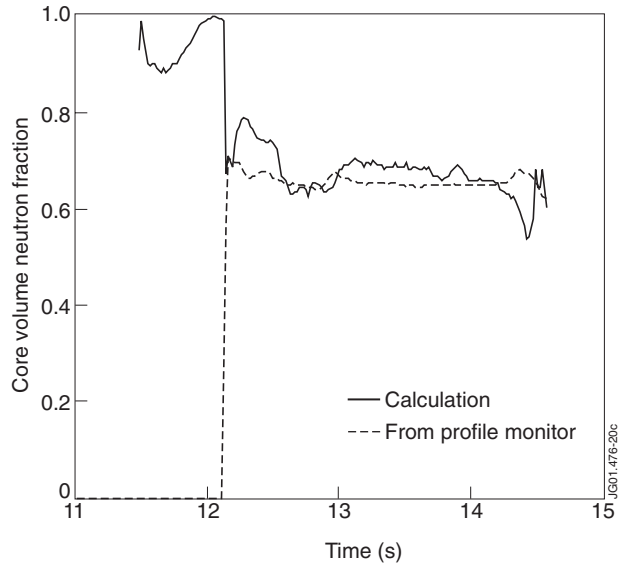

Fig. 20: The core neutron fraction corresponding to figs. 17-19. The dashed curve is obtained from the neutron profile analysis programme and fairly represents the experimental profile data, provided the neutron yield is sufficiently strong. The solid curve is the calculated fraction, which has to be engineered to fit the experimental result.

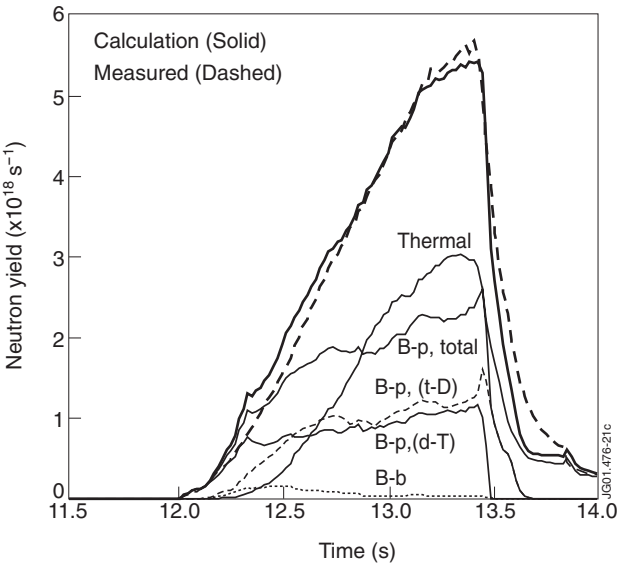

Fig. 21 : Breakdown of the neutron emission for Pulse No: 42976 into its component parts. The thick curve shows the calculated total neutron emission rate, to be compared with the measured rate (thick dashed curve). The thermal emission is shown, along with the total beam-plasma emission and the beam-beam emission. The total beam-plasma emission is further divided into d beams - T plasma and t beams - D plasma. A giant ELM occurred soon after termination of beam heating.

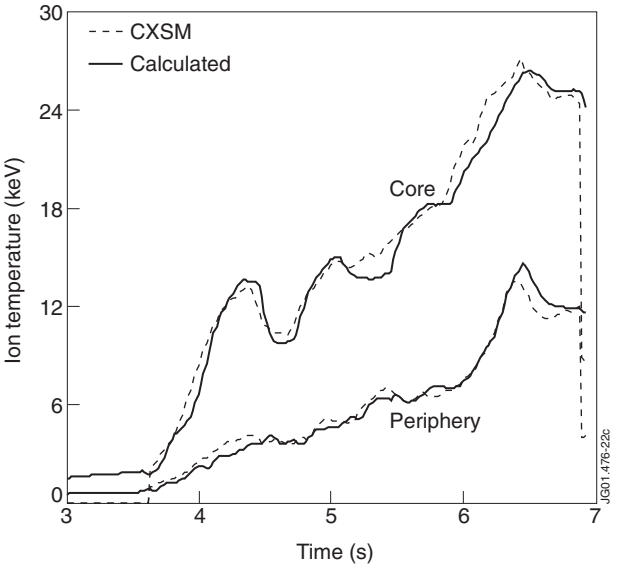

Fig. 22: Comparison of calculated and measured ion temperatures for Pulse No: 51976, a high performance optimised shear discharge in deuterium plasma.

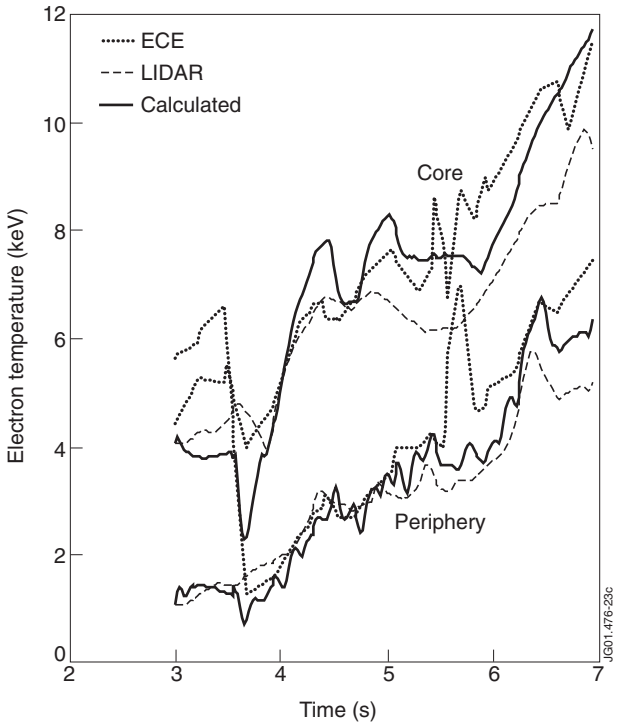

Fig. 23: Comparison of calculated and measured electron temperatures for Pulse No: 51976, a high performance optimised shear discharge in deuterium plasma. LHCD is applied for the first 0.5s.

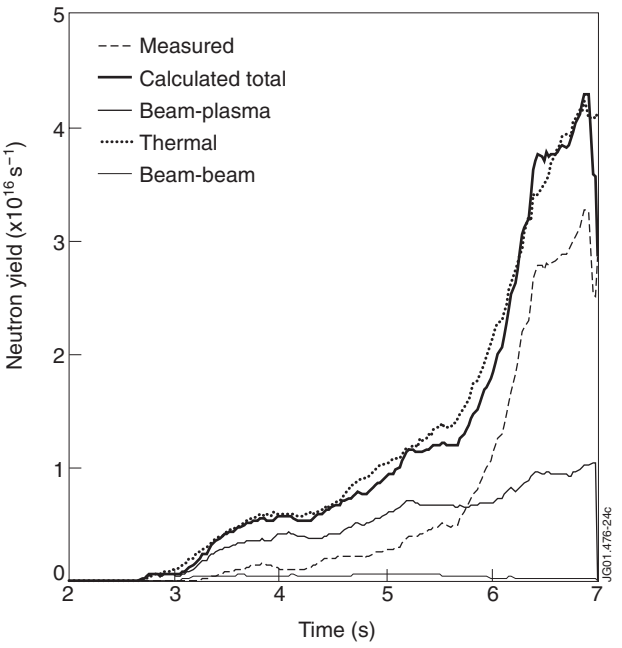

Fig. 24: Comparison of calculated and measured total neutron yields for Pulse No: 51976. At peak performance, the neutron emission is 75% thermal.

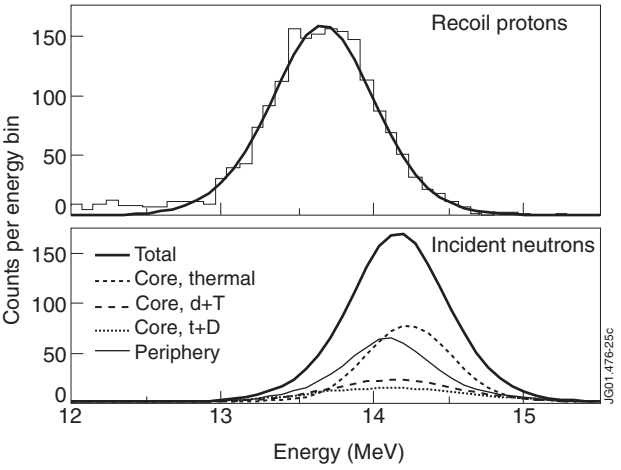

Fig. 25: Neutron energy spectrum for Pulse No: 42847, from 14.0 to 14.5s. The computed neutron energy spectrum is shown in the lower panel. There are several components to be considered. Core: passing 80keV and 142keV deuterons and 155keV tritons producing beam-plasma neutrons and a large 14keV thermal component. Periphery: single curve is a composite for nearly trapped 80 and 140keV deuterons and 155keV tritons producing beam-plasma neutrons and a 6keV thermal component. The plasma is rotating rapidly. The top panel shows the measured recoil proton energy spectrum compared with the computed neutron spectrum folded into the spectrometer response function, which does not allow for the low energy tail due to neutron down-scattering in the collimation. The spectrometer efficiency is considered a free parameter and the energy calibration is permitted to vary by up to 30keV.